TITLE: Neuronal identity control at the resolution of a single transcription factor isoform

AUTHOR NAMES AND AFFILIATIONS

- 4 Natalie Smolin¹, Mark Dombrovski^{2#}, Bryce W. Hina^{1#}, Anthony Moreno-Sanchez³, Ryan
- 5 Gossart⁴, Catherine R. Carmona⁴, Aadil Rehan², Roni H. Hussein², Parmis Mirshahidi², Jessica
- 6 Ausborn³, Yerbol Z. Kurmangaliyev*⁴, Catherine R. von Reyn*^{1,3}
- ¹ School of Biomedical Engineering, Science and Health Systems, Drexel University,
- 8 Philadelphia, PA

1

2

3

- 9 ² Howard Hughes Medical Institute, Department of Biological Chemistry, David Geffen School
- of Medicine, University of California, Los Angeles, CA
- ³ Department of Neurobiology and Anatomy, Drexel University College of Medicine,
- 12 Philadelphia, PA
- ⁴ Brandeis University, Department of Biology, Waltham, MA
- 14 # Equal Contribution
- *Correspondence:

15

19

20

21

22

23

- 17 yerbol@brandeis.edu
- 18 crv33@drexel.edu

25

26

27

28

29

30

31

32

33

34

35

36

37

38

39

40

41

42

43

44

45

46

Factors, Terminal Selector

SUMMARY The brain exhibits remarkable neuronal diversity which is critical for its functional integrity. From the sheer number of cell types emerging from extensive transcriptional, morphological, and connectome datasets, the question arises of how the brain is capable of generating so many unique identities. 'Terminal selectors' are transcription factors hypothesized to determine the final identity characteristics in post-mitotic cells. Which transcription factors function as terminal selectors and the level of control they exert over different terminal characteristics are not well defined. Here, we establish a novel role for the transcription factor broad as a terminal selector in Drosophila melanogaster. We capitalize on existing large sequencing and connectomics datasets and employ a comprehensive characterization of terminal characteristics including Perturb-seq and whole-cell electrophysiology. We find a single isoform *broad-z4* serves as the switch between the identity of two visual projection neurons LPLC1 and LPLC2. Broad-z4 is natively expressed in LPLC1, and is capable of transforming the transcriptome, morphology, and functional connectivity of LPLC2 cells into LPLC1 cells when perturbed. Our comprehensive work establishes a single isoform as the smallest unit underlying an identity switch, which may serve as a conserved strategy replicated across developmental programs. Keywords: Neurodevelopment, Neurobiology, *Drosophila melanogaster*, scRNA-seq,

Electrophysiology, Visual Projection Neurons, Visual System, Cell Identity, Transcription

INTRODUCTION

47

48

49

50

51

52

53

54

55

56

57

58

59

60

61

62

63

64

65

66

67

68

69

The determination of a neuron's identity—including the morphology, connectivity, and gene expression patterns that differentiate a neuronal cell—is a complicated task. Even within the humble fruit fly *Drosophila melanogaster*, more than 4,000 neural cell types (Scheffer et al., 2020; Schlegel et al., 2023) need to be determined, ensuring they exist in the appropriate space within the brain, establish their correct morphology, and connect to their intended partners, all within the volume of 5 nL (Makos et al., 2009). Our understanding of the regulatory logic required to specify unique and final neuronal identities is currently limited. Conserved across vertebrates and invertebrates alike, neural progenitors produce cell types based on their location and age. Both spatially restricted transcription factors and temporal cascades of transcription factors cooperate to determine which cell types are generated at what particular time during development (reviewed in (Chen & Konstantinides, 2022; Holguera & Desplan, 2018; Kumar, 2001). Within the medulla of *Drosophila melanogaster*, for example, a stereotyped cascade of specific transcription factors (Hth \rightarrow Ey \rightarrow Slp \rightarrow D \rightarrow Tll) pattern developing neuroblasts, and loss of Slp expression in the sequence can impede the generation of entire populations of cell types (Li et al., 2013). It is hypothesized that, in addition to transient transcription factor expression in progenitors, it is the persistent expression of certain transcription factors around the time of final mitosis throughout adulthood that specifies the terminal characteristics of a neuron (Allan & Thor, 2015; Hobert, 2008; Hobert, 2016; Holmberg & Perlmann, 2012). These 'terminal selectors' have been best studied in *C. elegans*, where selective removal or addition of transcription factors substantially altered the terminal characteristics, such as morphology and neurotransmitter type, that define neuron identity (Flames & Hobert, 2009; O'Meara et al., 2010;

71

72

73

74

75

76

77

78

79

80

81

82

83

84

85

86

87

88

89

90

91

92

Serrano-Saiz et al., 2013). Although evidence from *C. elegans* suggests a single terminal selector may be sufficient to define specific characteristics of identity, terminal selectors in larger animals are thought to act together in a combinatorial code (Allan & Thor, 2015; Arber et al., 1999; Hobert, 2016; Hobert & Kratsios, 2019; Tsuchida et al., 1994; Wolfram et al., 2014). To date, knowledge about which transcription factors serve as terminal selectors remains limited. Additionally, the extent to which one terminal selector affects multiple characteristics that define type identity has not been well explored. Terminal selector studies are often limited to quantifying one or two characteristics to assume an identity change, even though characteristics are not necessarily linked (Konstantinides et al., 2018). For example, although perturbations of individual terminal selectors can substantially alter cellular morphology, changes in morphology may not affect connectivity, as neuronal partners can adapt to find intended partners even when morphology is atypical (Valdes-Aleman et al., 2021). More comprehensive evaluations of terminal selectors are therefore needed to understand the extent to which terminal selectors exert their control. The *Drosophila* brain provides an excellent model for the study of terminal neuronal fate specification, due to its well-characterized, stereotyped wiring patterns and experimental tractability (Dorkenwald et al., 2022; Fischbach & Dittrich, 1989; Nern et al., 2015; Scheffer et al., 2020; Takemura et al., 2013; Takemura et al., 2015; Zheng et al., 2018). Electron microscopy datasets have enabled researchers to define the connectivity of a specific cell type (Dorkenwald et al., 2022; Nern et al., 2024; Scheffer et al., 2020; Schlegel et al., 2023; Zheng et al., 2018). Sophisticated genetic tools enable a 'plug-and-play' framework for inducing specific genetic perturbations exclusively in designated cell types (Dionne et al., 2018; Jenett et al., 2012; Lai & Lee, 2006; Perkins et al., 2015; Pfeiffer et al., 2010). Drosophila neurons are also amenable to

94

95

96

97

98

99

100

101

102

103

104

105

106

107

108

109

110

111

112

113

114

whole-cell electrophysiology, enabling the functional consequences of perturbations to be evaluated (von Reyn et al., 2014; von Reyn et al., 2017). And perhaps most critically, recent advancements within the field of transcriptomics allow tracking of genetic expression in a celltype-specific manner over the course of development, elucidating the temporal expression profile of specific genes (Davis et al., 2020; Konstantinides et al., 2018; Kurmangaliyev et al., 2020; Ozel et al., 2022; Ozel et al., 2021). One recent single-cell RNA sequencing (scRNA-seq) dataset of the developing fly optic lobes (Kurmangaliyev et al., 2020) has uncovered sustained differential 'on-off' expression of the transcription factor broad in two visual projection neuron cell types (VPNs) called lobula plate lobula columnar neuron type 1 (LPLC1) and lobula plate lobula columnar neuron type 2 (LPLC2) (Figure 1). VPNs detect specific visual features, with LPLC1 and LPLC2 encoding features of an object approaching on a direct collision course (Ache et al., 2019; Klapoetke et al., 2017; Klapoetke et al., 2022; Tanaka & Clark, 2022; von Reyn et al., 2017). LPLC1 and LPLC2 innervate the same brain regions, extending dendrites within the lobula and lobula plate of the optic lobes, and projecting axons out of the optic lobes and into the ventral lateral protocerebrum (VLP) in the central brain. Within these brain regions, LPLC1 and LPLC2 differ in dendrite and axonal targeting (Figure 1a,b). LPLC1 dendrites target layers 2-5B of the lobula (Lo2-5B) and layers 2-4 of the lobula plate (LoP2-4), while LPLC2 dendrites target Lo4-5B and Lop1-4. LPLC1 and LPLC2 axons terminate in their own, separate glomeruli within the VLP. The resolvable differences in morphology along with the genetic accessibility of LPLC1 and LPLC2 make these cell types promising for investigating broad as a potential terminal selector that may differentiate the two cell types.

In *Drosophila*, the transcription factor *broad* has been well studied as having a key role during fly metamorphosis, and is necessary for the transition from larvae to pupae (Bayer et al., 1996; Karim et al., 1993; Restifo & White, 1991). *Broad* is expressed across tissues in the prepupal stages, induced through the global ecdysone hormone cascade that drives metamorphic events (Bayer et al., 1996; Brennan et al., 2001; Emery et al., 1994; Huet et al., 1993; Mugat et al., 2000; Zhou et al., 2009). *Broad* has also recently been implicated in the early cell patterning of type II neuroblasts (El-Danaf et al., 2023), working as a temporal transcription factor. Despite being well studied within the early stages of pupal development, very little is known of its ability to terminally differentiate cells.

Here, we investigate the role of the transcription factor *broad* as a terminal selector that differentiates two closely related VPNs during development, evaluating putative changes in cellular identity that result through perturbations of this program. Through the knock-down of *broad* in LPLC1 cells and the overexpression of *broad* in LPLC2 cells, we investigate morphological changes that indicate altered terminal identity. We establish differences between LPLC1 and LPLC2 synaptic partners using connectome datasets and use whole-cell patch clamp electrophysiology and optogenetics to determine how perturbing *broad* expression alters synaptic partner specificity and functional connectivity. Finally, we perform single-cell RNA sequencing after *broad* perturbation to evaluate the impact of individual *broad* isoforms on transcriptional identity. Our work elucidates mechanisms that define terminal cellular identity, establishing a role for *broad* as a terminal selector and revealing a minimal unit required to distinguish final and unique cell type identity.

RESULTS

broad is differentially expressed between LPLC1 and LPLC2.

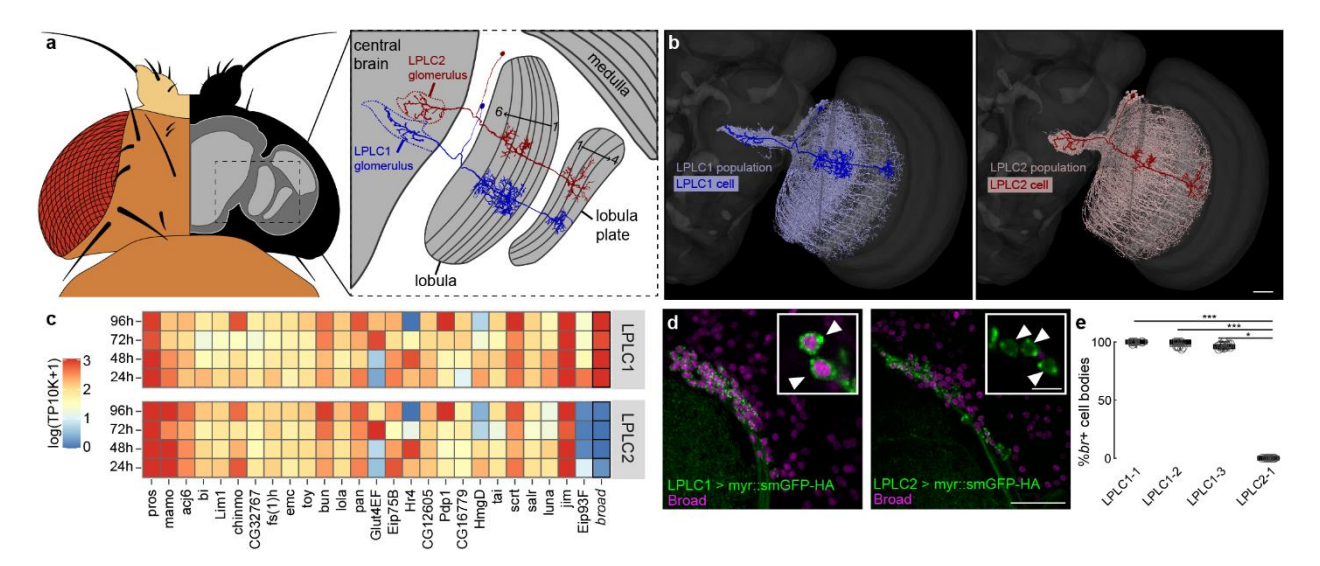


Figure 1: The transcription factor *broad* is differentially expressed between LPLC1 and LPLC2.

- (a) Fly brain schematic dorsal view illustrating single LPLC1 and LPLC2 neuron projection patterns.
- (b) Mesh reconstruction (Dorkenwald et al., 2022) of LPLC1 (left) and LPLC2 (right) populations within
 an anterior view of the fly brain. A single LPLC1 (left) and LPLC2 (right) drawing has been overlaid onto
 these populations.
 - (c) Heatmaps showing expression of transcription factors in developing LPLC1 and LPLC2 neurons, data from (Kurmangaliyev et al., 2020). Columns are highly expressed genes that define these two cell-types, and rows indicate hours after pupae formation (APF). The average normalized expression is shown as log-transformed TP10K values (transcripts-per-10,000 UMI). See Methods for details.
 - (d) Broad protein labeling displaying *broad* positive LPLC1 cell bodies (left) and *broad* negative LPLC2 cell bodies (right). Scale bar = $20 \mu m$. Insets feature a zoomed in single plane with arrowheads pointing to individual cell bodies. Inset scale bar = $5 \mu m$.
 - (e) Quantification of *broad* positive somata in three LPLC1 driver lines and one LPLC2 driver line. $N \ge 6$ animals for all conditions. Kruskal Wallis (p = 7.31e-8), Dunn-Sidak post hoc. * = p<0.05, ** = p<0.01,

155 *** = p < 0.001.

138

139

140

141

142

146

147

148

149

150

151

152

153

154

157

158

159

160

161

162

163

164

165

166

167

168

169

170

171

172

173

174

175

176

177

178

To identify candidate terminal selectors that may control differential terminal characteristics between LPLC1 and LPLC2, we referenced the scRNA-seq transcriptional atlas of the D. melanogaster visual system (Kurmangaliyev et al., 2020) and identified all transcription factors that are highly expressed in the developing LPLC1 and LPLC2 neurons (Figure 1c). Only two transcription factors, Eip93F and *broad*, were differentially expressed between these two cell types. However, only *broad* had an 'on-off' expression pattern that was maintained throughout development (Figure 1c), giving us reason to believe *broad* may help differentiate these two cell types. The time points 24-96 hours after pupal formation (h APF) are when LPLC1 and LPLC2 establish their morphology and wire into circuits (McFarland et al., 2024). We therefore hypothesized that *broad* is a key factor in differentiating LPLC1 from LPLC2, acting as a terminal selector to establish LPLC1 identity. We then validated that broad protein expression patterns matched the on-off mRNA expression patterns from scRNA-seq data with immunolabeling, confirming broad was only expressed in LPLC1 cell bodies (Figure 1d,e). Changes in broad expression induce morphological changes in LPLC1 and LPLC2. If broad is acting as a terminal selector to differentiate LPLC1 from LPLC2, perturbations in *broad* expression should directly impact the wiring programs of these cells, for instance, causing LPLC1 to resemble LPLC2. To investigate our terminal selector hypothesis, we knocked down broad in LPLC1 using two different RNAi lines that target all broad isoforms (Perkins et al., 2015). We found both broad knock-down conditions led to alterations in LPLC1 axon morphology and targeting. The total volume occupied by axon terminals for the broad RNAi-1

condition increased slightly (Figure 2a,b), suggesting that these axons are occupying more space, extending outside of the LPLC1 glomerulus region. Surprisingly, we observed a decrease in total volume occupied by axon terminals for the *broad* RNAi-2 condition (Figure 2a,b), accompanied by an overall decrease in the number of LPLC1 somata (Supplementary Figure 1). We reasoned this decrease may occur because a portion of perturbed neurons are no longer fully being recognized by the LPLC1 driver line when *broad* expression is decreased. We found fluorescence within the LPLC1 glomerulus was not significantly changed after *broad* knockdown in LPLC1 (Figure 2c,d). Both knock-down conditions did however lead to LPLC1 axonal tracts targeting the LPLC2 glomerulus (Figure 2e,f). These data suggest *broad* expression in LPLC1 establishes its axon morphology, and the loss of *broad* in LPLC1 redirects its axons towards LPLC2 targets.

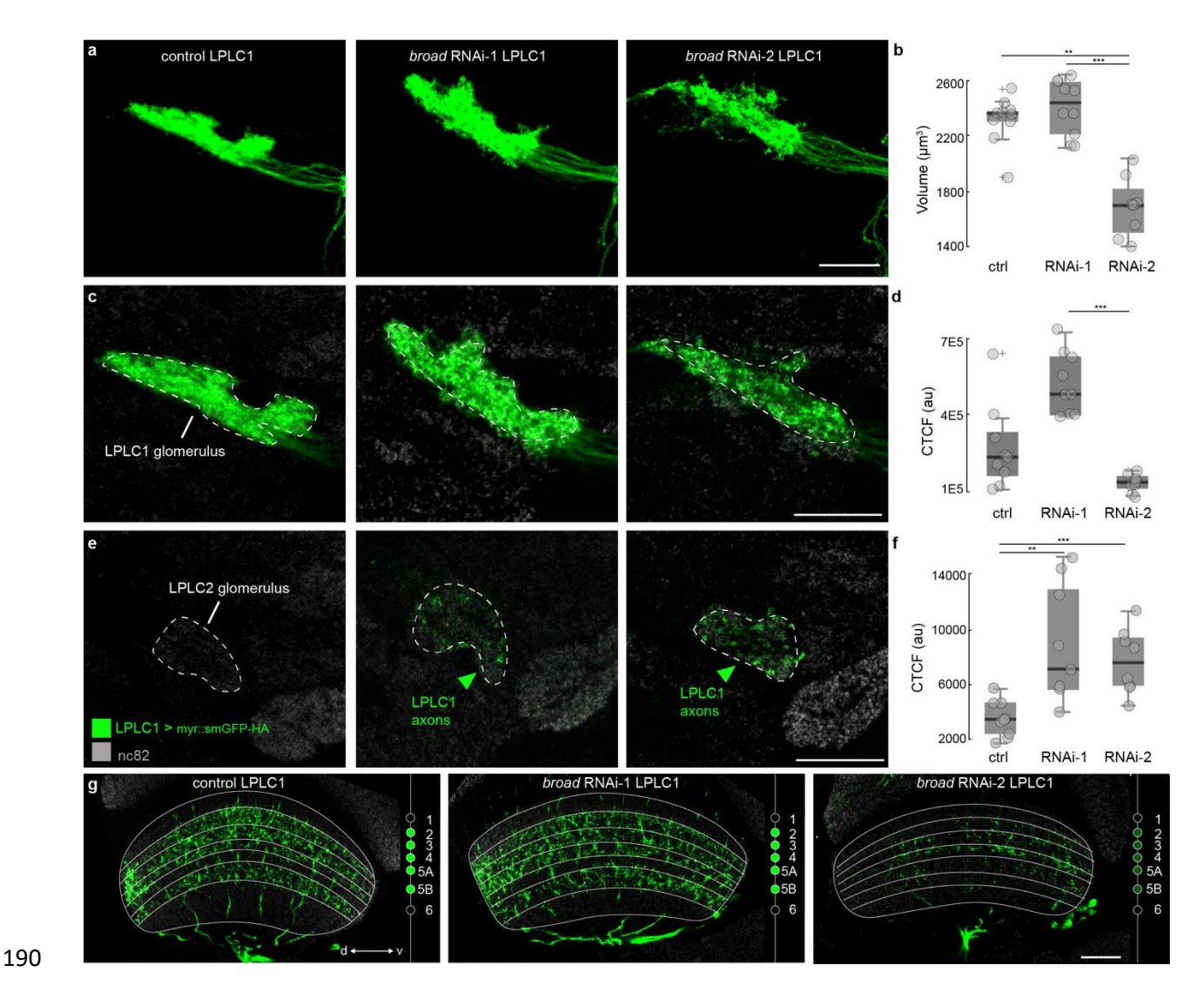


Figure 2: Knock-down of *broad* in LPLC1 cells results in ectopic axonal branching into the LPLC2 glomerulus.

- (a) Maximum projection images of axons tracts for control LPLC1 and *broad* knock-down (*broad* RNAi-1 and *broad* RNAi-2) LPLC1 cells. Scale bar = 20 μm.
- 195 **(b)** Quantification of overall axonal volume of each condition in **(a)**. $N \ge 4$ animals for each condition.
- 196 Kruskal Wallis (p = 2.98e-04), Dunn-Sidak post hoc. * = p<0.05, ** = p<0.01, *** = p<0.001.

192

193

194

198

20 μm.

197 (c) Single plane images depicting the innervation of the LPLC1 glomerulus by LPLC1 axons. Scale bar =

199 (d) Quantification of LPLC1 axon density (corrected total cell fluorescence, CTCF) in the LPLC1 200 glomerulus shown in (c). $N \ge 4$ animals for each condition. Kruskal Wallis (p = 1.84e-04), Dunn-Sidak post hoc * = p < 0.05, ** = p < 0.01, *** = p < 0.001. 201 202 (e) Single plane images depicting the innervation of the LPLC2 glomerulus by LPLC1 axons. Scale bar = 203 20 μm. (f) Quantification of LPLC1 axon density (CTCF) in the LPLC2 glomerulus shown in (e), N > 4 animals 204 205 for each condition. Kruskal Wallis (p = 0.0053), Dunn-Sidak post hoc *= p<0.05, ** = p<0.01, ***= 206 p<0.001. Scale bar = 20 μ m. We note we did not witness a full targeting switch for the axons, which could be due to 207 physical competition with LPLC2 for space on postsynaptic partners (McFarland et al., 2024). 208 We also witnessed no morphological changes to LPLC1 dendrites with broad knock-down 209 210 (Figure 2g), which could signify a limiting time-lag between RNAi expression and subsequent protein knock-down (Yao et al., 2015). Terminal selectors are thought to require early and 211 sustained expression across development, and as our split-GAL4 LPLC1 line turns on at around 212 213 12h-24h APF (McFarland et al., 2024), these RNAi tools may not start working early enough to 214 completely alter axon targeting and dendrite morphology.

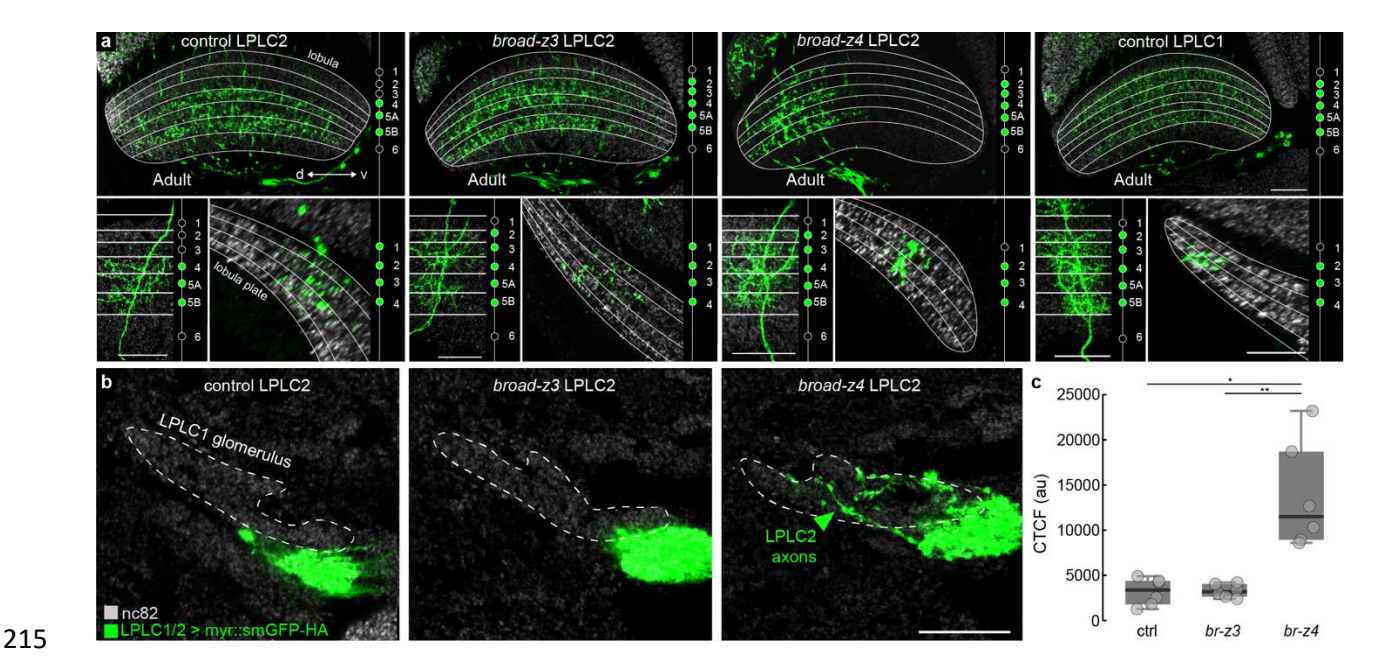


Figure 3: *broad-z3* and *broad-z4* overexpression in LPLC2 cells result in LPLC1-like morphologies.

- (a) (top) Innervation of the lobula for control LPLC2 cells, broad-z3 LPLC2 cells, broad-z4 LPLC2 cells, and control LPLC1 cells. Scale bar = $20~\mu m$. (bottom left) Single cell morphology of cells within the lobula. Scale bar = $20~\mu m$. (bottom right) Single cell morphology of cells within the lobula plate. $N \ge 6$ animals for each condition. Scale bar = $20~\mu m$.
- **(b)** Innervation of the LPLC1 glomerulus for control, *broad-z3*, and *broad-z4* LPLC2 cells.
- (c) Quantification of LPLC2 axon density (CTCF) in the LPLC1 glomerulus shown in (b). $N \ge 6$ animals for each condition. Kruskal Wallis (p = 0.0034), Dunn-Sidak post hoc * = p<0.05, ** = p<0.01, *** = p<0.001. Scale bar = 20 μ m.

Based on our finding that the knock-down of *broad* changes LPLC1 axonal projection targeting towards LPLC2 targets in the central brain, we next investigated whether the overexpression of *broad* could alter the morphology of LPLC2 to resemble LPLC1. We expressed individual isoforms of *broad* in LPLC2 and found only two (*broad-z3* and *broad-z4*) affected LPLC2 morphology (Figure 3 and Supplementary Figure 2). At the level of the

232

233

234

235

236

237

238

239

240

241

242

243

244

245

246

247

248

249

250

251

252

dendrites, LPLC2 innervates layers 4-5B of the lobula, but broad-z3 or broad-z4 overexpression resulted in dendritic innervation across layers 2-5B of the lobula, which is the typical innervation pattern of LPLC1 (Figure 3a) (Wu et al., 2016). To better resolve individual morphologies, we used the MultiColor FlpOut (MCFO) technique (Nern et al., 2015) to sparsely label control LPLC1 cells, control LPLC2 cells, broadz3 LPLC2 cells and broad-z4 LPLC2 cells (Figure 3a). As observed when labeling the full population, we found at the single cell level broad-z3 and broad-z4 overexpression in LPLC2 cells caused the lobula dendrites to exhibit LPLC1-like morphology. Sparse labeling also enabled us to resolve dendrite arborization patterns in the lobula plate. We found control LPLC2 cells to arborize in LoP1-4 and control LPLC1 cells to arborize in LoP2-4 (Figure 3a), consistent with current literature (Tanaka & Clark, 2022; Wu et al., 2016). Furthermore, we found that only broad-z4 changed LPLC2 dendritic innervations pattern within the lobula plate to LoP2-4, resembling LPLC1 dendrites. We next investigated how broad-z3 and broad-z4 overexpression changes the axonal morphology of LPLC2 cells. We found broad-z4 LPLC2 axons innervated the LPLC1 glomerulus (Figure 3b,c), suggesting the expression of *broad-z4* is sufficient to redirect LPLC2 axons towards LPLC1 postsynaptic targets. Overall, broad-z4 demonstrated the most significant alterations in terminal LPLC2 morphology across the lobula, lobula plate, and axonal terminals. We also note that *broad-z4* overexpression in adult LPLC2 cells consistently appeared to lead to a loss of dendrites in the dorsal half of the lobula and lobula plate (Figure 3a), and a decrease in the overall number of LPLC2 somata. Upon further examination, however, we found the "missing" population was weakly labeled by the LPLC2 driver line, indicating the driver line

may have difficulty recognizing these perturbed cells as still being LPLC2 (Supplementary

Figure 3).

253

254

255

256

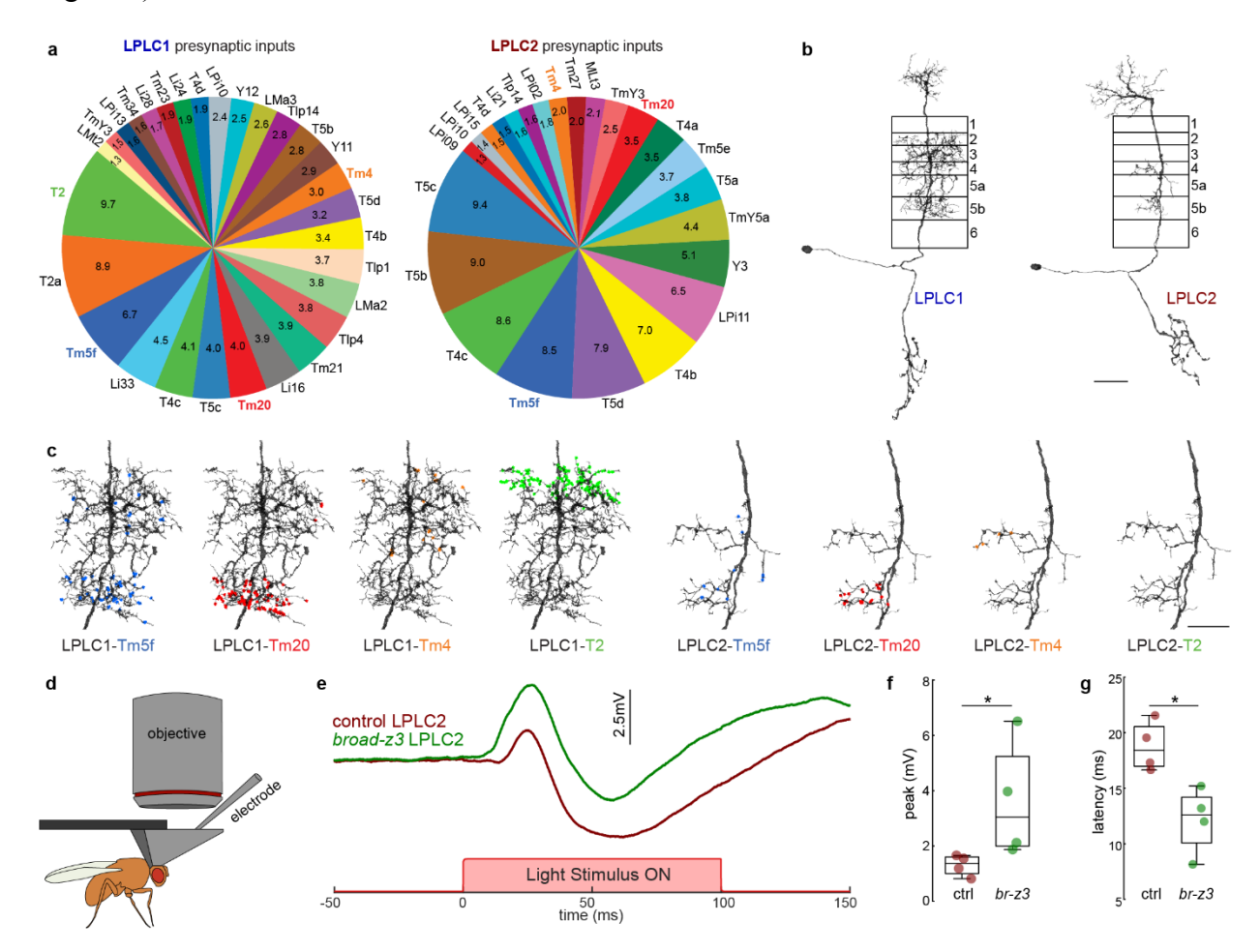


Figure 4: T2 cells are now connected to LPLC2 cells with the overexpression of broad.

- 257 (a) Presynaptic inputs greater than 1% of total synapse counts to LPLC1 and LPLC2.
- 258 **(b)** Mesh reconstruction (Dorkenwald et al., 2022; Schlegel et al., 2023; Zheng et al., 2018) of a
- representative (left) LPLC1 or (right) LPLC2 neuron. Approximate lobula layers have been boxed over
- 260 the dendrites. Scalebar = $15 \mu m$.
- 261 (c) Mesh reconstructions of all synapses (colored circles) from Tm5f, Tm20, Tm4, and T2 neurons
- (Buhmann et al., 2021; Dorkenwald et al., 2022; Heinrich et al., 2018; Schlegel et al., 2023; Zheng et al.,
- 263 2018) on a (left) LPLC1 and a (right) LPLC2 neuron. Scalebar = 10 μm.

265

266

267

268

269

270

271

272

273

274

275

276

277

278

279

280

281

282

283

284

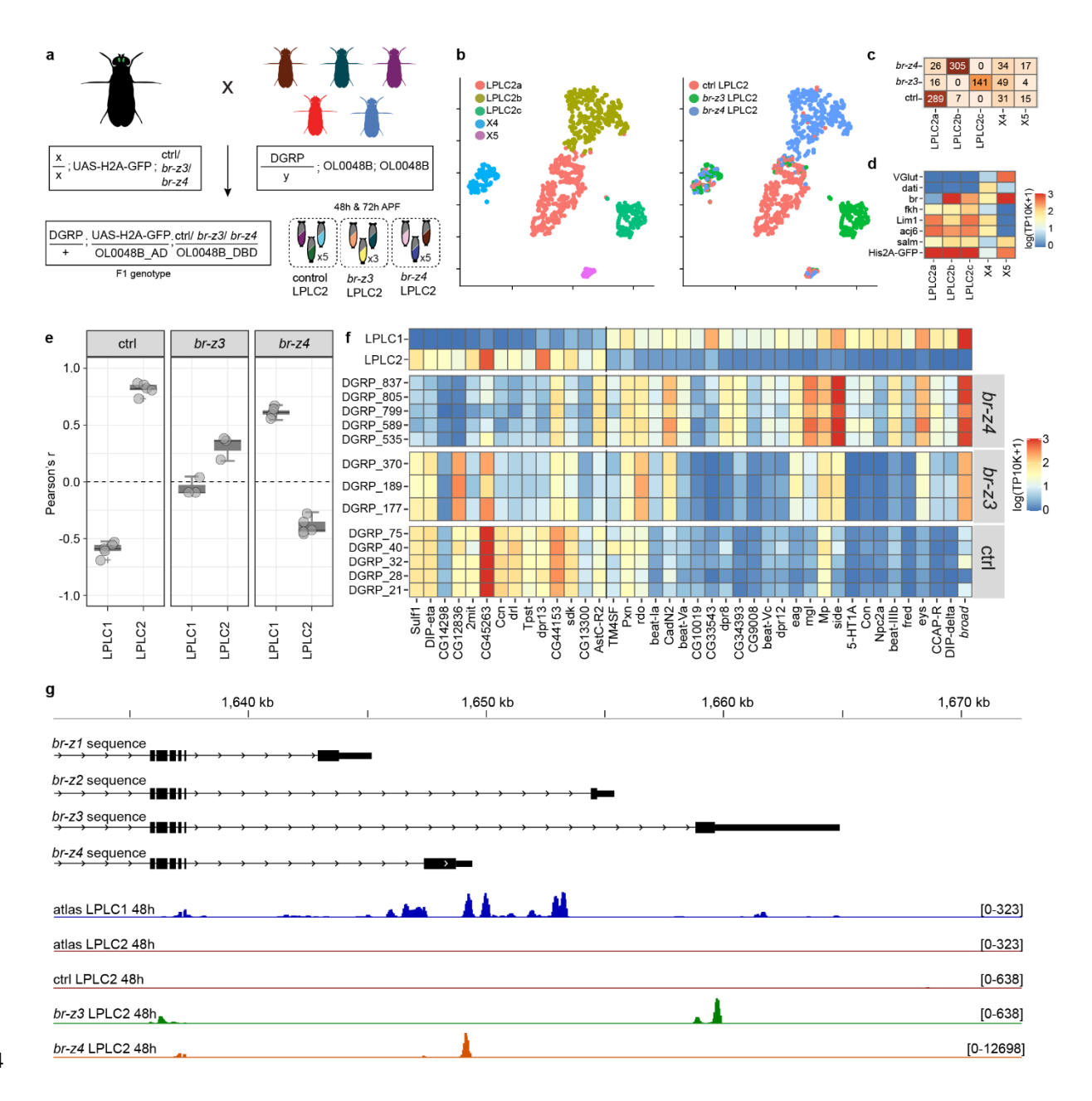
285

286

287

(d) Schematic illustrating whole-cell electrophysiology and optogenetics setup with light delivery through the objective. (e) Average responses for LPLC2 with and without *broad* isoform overexpression when T2 are optogenetically activated. (\mathbf{f},\mathbf{g}) Quantification of (\mathbf{f}) peak depolarization and (\mathbf{g}) activation latency. N=4 animals for each condition. Wilcoxon Rank Sum Test, * = p < 0.05. LPLC2 cells have altered connectivity resulting from broad overexpression. The observed alterations in layer specific dendrite targeting suggest there may be a change in synaptic partners that occurs when *broad* is expressed in LPLC2, with LPLC2 receiving inputs from lobula or lobula plate cell types normally reserved for LPLC1. To establish which changes in synaptic partners could occur with broad expression, we used the Full Adult Fly Brain (FAFB) electron microscopy (EM) dataset (Dorkenwald et al., 2022; Zheng et al., 2018), to determine the presynaptic inputs for LPLC1 and LPLC2 (Figure 4a). While we found Tm5f, Tm20, and Tm4 (Supplementary Figure 5) to provide strong inputs to both LPLC1 and LPLC2 populations, we found T2 cells to provide one of the largest differences in lobula presynaptic inputs between LPLC1 and LPLC2 (Figure 4a,c). T2 neurons form synapses with LPLC1 in layers 2 and 3 of the lobula, but do not provide a major synaptic input to LPLC2. Since LPLC2 that overexpress broad-z3 and broad-z4 show novel dendritic innervations in layers 2 and 3 of the lobula, we hypothesized *broad* expressing LPLC2 may be forming direct, functional synapses with T2 in these layers. To investigate whether these putative synapses between T2 and broad expressing LPLC2 were functional, we combined optogenetic activation of T2 with whole-cell electrophysiology recordings from LPLC2 to assess direct synaptic coupling (Figure 4d,e). From these recordings,

we found that LPLC2 cells expressing *broad-z3* have a significantly larger depolarization when T2 cells are optogenetically activated, as compared to control LPLC2 cells (Figure 4e,f). We also find *broad-z3* LPLC2 responses exhibit a shorter latency than control responses, suggesting direct synaptic coupling (Figure 4e,g). Our results suggest that the overexpression of *broad-z3* is sufficient to change connectivity in LPLC2 cells, and that LPLC2 cells are now functionally connected to T2 cells.



296

297

298

299

300

301

302

303

304

305

306

307

308

309

310

311

312

313

314

315

316

317

318

319

Figure 5: Overexpression of broad-z4 recodes transcriptional identities of LPLC2 cells. (a) Experimental design of the multiplexed single-cell Perturb-Seq experiment. F1-generation of pupae carry the LPLC2 split-Gal4 driver (OL0048B), a nuclear GFP reporter (UAS-H2A-GFP), an overexpression or control construct (ctrl, broad-z3, broad-z4), and a replicate-specific wild-type Xchromosome (DGRP). LPLC2 neurons were purified and used for scRNA-seq at two timepoints (48h and 72h APF). Each experimental condition was replicated 3-5 times. The analysis at 48h APF is shown in (bg); the analysis at 72h APF is shown in Supplementary Figure 4. See Methods for more details. (b) t-distributed stochastic neighbor embedding (tSNE) plots are used only for visualization of the clustering of the data. Left, cells are color coded based on unsupervised clustering; Right, cells are color coded based on experimental conditions. (c) Cell counts across clusters and conditions. (d) Expression levels of LPLC2-specific transcription factors (Kurmangaliyev et al., 2020; Ozel et al., 2022) nuclear GFP reporter, and two genes enriched in ectopic, non-LPLC2, clusters (X4/X5). (e) Correlation analysis between transcriptional profiles of LPLC1 and LPLC2 neurons from the developmental atlas (Kurmangaliyev et al., 2020) and LPLC2 neurons in each experimental condition. Comparisons are based on differentially expressed genes (DEGs) between LPLC1 and LPLC2 from (f). Circles are Pearson's r for individual replicates; boxplots are distributions. (f) Heatmaps of expression patterns of DEGs between LPLC1 and LPLC2 at 48h APF. Expression patterns are shown in the atlas (top) and for each condition and replicate. DGRP lines for each X chromosome and replicate are indicated. See Methods for thresholds. (g) Coverage plots of scRNA-seq reads at the 3'-UTR region of broad in the atlas and Perturb-seq datasets. Most of the reads support the expression of the broad-z4 isoform in LPLC1 neurons. Note that coverage of the overexpression constructs is restricted to the coding regions of corresponding transcripts.

broad-z4 recodes transcriptomes of LPLC2 cells into LPLC1-like cells.

321

322

323

324

325

326

327

328

329

330

331

332

333

334

335

336

337

338

339

340

341

342

Our data to this point suggest broad establishes aspects of morphology and functional connectivity of LPLC1 cells, distinguishing them from LPLC2, as predicted if broad is acting as a terminal selector. One outstanding question of terminal selectors is to what extent they determine identity. Do they only serve to control a subset of terminal characteristics, or do they have the capacity to fully switch cell type identity? We therefore investigated whether broad's control extended beyond morphology to change the transcriptional profile of LPLC2 to resemble LPLC1. To investigate to what extent *broad* determines neuronal identity, we performed a single-cell RNA sequencing experiment of purified LPLC2 cells in wild-type (control) and broad overexpression conditions (Perturb-seq). To minimize technical variation between experimental conditions, we leveraged a genetic multiplexing strategy using wild-type chromosomes from the Drosophila Genetic Reference Panel (DGRP) strains as molecular tags for individual replicates (Figure 5a) (Huang et al., 2014; Kang et al., 2018; Mackay et al., 2012). This strategy was previously used for high-throughput multiplexed profiling of developmental trajectories of neurons (Kurmangaliyev et al., 2020) and genetic perturbations of neurons (Jain et al., 2022). We purified and sequenced LPLC2 cells overexpressing broad-z3, broad-z4, and a control genotype at 48h and 72h APF (Figure 5, Supplementary Figure 4), as many aspects of cell type identity and wiring patterns are established at these stages of development (Kurmangaliyev et al., 2020; McFarland et al., 2024). Overexpression of the two different broad isoforms resulted in two transcriptionally distinct populations of LPLC2 neurons indicating significant and distinct transcriptional effects of each isoform (Figure 5b-d, Supplementary Figure 4a-c). Next, we compared expression profiles of broad-expressing LPLC2 neurons to wild-type LPLC1 and LPLC2 neurons obtained from the developmental atlas of the *Drosophila* visual

system (Kurmangaliyev et al., 2020). The correlation analysis based on differentially expressed genes between LPLC1 and LPLC2 revealed distinct effects of the *broad* isoforms (Figure 5e-f). Transcriptomes of *broad-z3* LPLC2 neurons differed from both wild-type LPLC1 and LPLC2 neurons, but were more similar to wild-type LPLC2 neurons. In contrast, *broad-z4* LPLC2 neurons became more similar to wild-type LPLC1 than wild-type LPLC2 neurons. Taken together, our data suggest that *broad-z4* acts as a terminal selector between developing LPLC1 and LPLC2 cells, and acts as a key determining factor that establishes final transcriptional cell identity during these late-stages of neuronal development.

Given that our Perturb-seq data implicate *broad-z4* in switching identity between LPLC1 and LPLC2, we investigated what isoform is present natively in control LPLC1 cells. The *broad* gene is comprised of four isoforms, linking a common 5' N-terminal to one of four pairs of 3' zinc fingers. Since the atlas of the developing visual system generated 3' RNA reads, we were able to determine which *broad* isoforms are expressed in each cell type. Four annotated isoforms of *broad* differ by zinc-finger domains encoded by alternative exons at 3'-UTR of the gene (Gramates et al., 2022). Excitingly, the analysis of scRNA-seq reads coverages in wild-type datasets showed that LPLC1 cells only express the *broad-z4* isoform (Figure 5g). These data corroborate our morphological studies, as *broad-z4* is the only isoform that induces morphological changes of LPLC2 at both their axons and dendrites. Our data suggest that while *broad* may be the distinguishing transcription factor between LPLC1 and LPLC2, the regulatory control it exerts is at the level of the isoform, and the differences between LPLC1 and LPLC2 cells are controlled by the *broad-z4* isoform.

DISCUSSION

367

368

369

370

371

372

373

374

375

376

377

378

379

380

381

382

383

384

385

386

387

388

Terminal selector genes are thought to establish the terminal characteristics that define final cell identities (Hobert, 2008; Hobert, 2016). Final identity often requires a unique combinatorial expression of terminal selectors to implement all terminal characteristics (Allan & Thor, 2015; Hobert, 2016; Ozel et al., 2022). In this work, we elucidate one gene, broad, that is able to act as a terminal selector to differentiate neuronal identity between LPLC1 and LPLC2 cells through morphological, transcriptomic, and functional connectivity changes. Delving further, we find this control is exerted at the level of a single isoform, and that *broad-z4* is capable of fully switching the identity of LPLC2 cells. We demonstrate a novel role for *broad*, working as a terminal selector to establish final and unique cellular identities within the fly visual system. *Broad* is best known to ensure appropriate stage-specific responses to hormone signaling during metamorphosis (Karim et al., 1993). Null mutations and deletions of broad lead to lethality at the end of the larval stage, indicating the requirement of broad for normal fly metamorphosis (Belyaeva et al., 1980; Kiss et al., 1988; Kiss et al., 1976; Restifo & White, 1991). More recent works have implicated broad as a temporal transcription factor, working in a cascade to pattern developing type II neuroblasts (El-Danaf et al., 2023). Through both temporal and spatial patterning, the nervous system is able to re-use the same genes in different contexts to allow a brain to overcome the wiring problem inherent to a brain—the idea that the number of connections in a brain outnumber the number of genes it has by several orders of magnitude (Hassan & Hiesinger, 2015). The function of broad as a terminal selector may be specific in converting LPLC2 into LPLC1 neurons, but *broad* may be capable of acting as a terminal selector across multiple cell types. Future work should investigate whether broad exerts control over the same terminal characteristics and utilizes the same mechanisms to exert its control.

390

391

392

393

394

395

396

397

398

399

400

401

402

403

404

405

406

407

408

409

410

411

We find broad's terminal selector effects are specific to the individual broad isoform. Broad encodes four major protein isoforms, *broad-z1*, -z2, -z3, and -z4. These isoforms share a common animo-terminal core region but differ in their carboxy-terminal Zn fingers (Bayer et al., 1997; DiBello et al., 1991). Broad, formerly called Broad-Complex or BR-C, is known to encode for three functions throughout the *Drosophila* central nervous system: br (broad), rbp (reduced bristle number on palpus), and 2Bc (Belyaeva et al., 1980; Kiss et al., 1988). All three functions control aspects of CNS reorganization: br^+ is required for leg and wing imaginal disc morphogenesis and tanning and hardening of the larval cuticle, rbp^+ is required for muscle and bristle development, $2Bc^+$ is required for the closure of the thoracic epidermis (Bayer et al., 1997; Crossgrove et al., 1996). The br function is thought to be provided by the -z2 isoform, the *rbp* function by the -z1 and -z4 isoforms, and the 2Bc by the -z3 isoform (Bayer et al., 1997). Here we define an additional, novel role for the *broad-z4* isoform as a terminal selector of LPLC1 cells. *Broad-z4* is the isoform present in native LPLC1 cells (Figure 5g) and perturbations of broad-z4 result in the most significant switching of LPLC2 to LPLC1-like morphology at both the axons and the dendrites of these cells (Figure 3), as well as an LPLC1like switch in transcriptional identity (Figure 5). Interestingly, broad-z3 also seems to have an effect on changing LPLC2 morphology and gene expression profiles, albeit to a lesser extent. Previous studies have indicated that there may be partial functional redundancy among the different *broad* isoforms. One type of rbp mutant (resulting in reduced bristle numbers) are fully rescued by the -z1 broad isoform but also partially rescued by the -z4 broad isoform (Bayer et al., 1997). Similarly, 2Bc lethality can be rescued by broad-z3 protein expression, but also partially rescued by broad-z2 protein expression (Bayer et al., 1997). Here, we support these past findings that different *broad* isoforms have

413

414

415

416

417

418

419

420

421

422

423

424

425

426

427

428

429

430

431

432

433

434

functional redundancies, but in a new context. In addition to the hydrophobic residues, cysteines, and histidines present in all C2H2 zinc-finger proteins (Miller et al., 1985), there is a high degree of similarity within the different zinc-finger domains (Bayer et al., 1996). The DNA binding domain of the -z3 isoform, for instance, is quite similar to that of the -z4 isoform (Bayer et al., 1996), and the redundancy that we see between the two isoforms could be based on structural similarity. Broad-z4, however, is the only isoform with a 5' untranslated sequence of cDNA that diverges from the core sequence at position 163 kb (Bayer et al., 1996). This sequence specific to the -z4 isoform may be part of the reason why the -z4 isoform has such strong effects on changing terminal identity of LPLC2 cells. Previous studies have also found terminal selectors to act at the level of the isoform, however these studies have often focused their investigations on only a few aspects of terminal identity such as morphology, neurotransmitter identity, and the altered expression of downstream genes (Ahn et al., 2022; Campbell & Walthall, 2016; Chu et al., 2024; Neville et al., 2014; Pereira et al., 2019; Remesal et al., 2020). Here, we quantitatively demonstrate how a terminal selector results in functional changes in synaptic specificity, expanding beyond changes in morphology and gene expression that have been a common read out for terminal selectors. Overexpression of an LPLC1 terminal selector, broad, in LPLC2 cells causes them to be synaptically coupled to T2 cells, which are LPLC1specific synaptic partners. We anticipate broad-LPLC2 cells would have different visual tuning, as they now receive novel visual information, and would demonstrate responses matched to LPLC1 tuning for visual stimuli such as small moving squares or back-to-front motion (Klapoetke et al., 2022; Tanaka & Clark, 2022). Terminal selectors are thought to activate cell-type specific effector genes that define the final differentiated identity of a mature neuron (Hobert & Kratsios, 2019). Differentially

expressed genes from our Perturb-seq experiment may give insights as to target genes where *broad* exerts its regulatory control. Loss of *broad* results in altered expression of numerous genes, including cellular adhesion molecules that control synaptic specificity, as seen in our own Perturb-seq dataset. Other studies have found loss of a terminal selector to result in changes in gene expression including TFs, GPCRs, and ion channels (Hobert, 2016; Ozel et al., 2022; Wyler et al., 2016). Further chromatin binding studies such as ChiP-seq or DamID-seq would be required to definitively determine what downstream targets *broad* regulates.

Work in C. elegans has proposed terminal selectors for 98/118 neuron classes (Hobert, 2021), yet in other invertebrates and vertebrates, terminal selectors have bene identified in very few cell types. Our identification here of a terminal selector that specifies unique and final cell identities provides the most in-depth characterization of changes in identity that result from perturbing a terminal selector. The methodology here may also serve as a general framework as to how terminal selectors may be identified and evaluated in the future. The identification of terminal selectors enables further investigations into the mechanisms, downstream of terminal selectors, by which final cell identity characteristics are established. A failure to appropriately establish identity and maintain terminal characteristics may underlie neurodevelopmental and neuropsychiatric disorders, and many terminal selectors have orthologs in humans that have been involved in these disease states (Chao et al., 2017; Deneris & Hobert, 2014; Sahay & Hen, 2007; Sleven et al., 2017). In fact, the human ortholog of *broad* is BTBD18, and the genetic loci where it resides has recently been discovered to be linked to schizophrenia (Schizophrenia Working Group of the Psychiatric Genomics, 2014). The future impact of this work may therefore yield strategies to resolve or redefine neuronal identity in a clinical setting.

435

436

437

438

439

440

441

442

443

444

445

446

447

448

449

450

451

452

453

454

455

456

MATERIALS AND METHODS

Fly Stocks and developmental staging

Drosophila melanogaster were reared on a standard molasses, cornmeal, and yeast diet (Archon Scientific) and kept at 25°C and 60% humidity on a 12-hour light/dark cycle throughout development. For optogenetics experiments, larval flies were raised in the dark on low retinal food (standard food plus 0.2 mM retinal) and switched to high retinal food (standard food plus 0.4 mM retinal) upon eclosion. For developing pupal experiments, white pre-pupae (0h APF) were collected and incubated for the indicated number of hours. All experiments were performed on staged pupae or adult female flies 2-5 days post-eclosion. Fly genotypes are listed in Supplemental Table 1.

Visualization of single-cell morphology

To visualize single cells of LPLC1 and LPLC2, we used MultiColor FlpOut (MCFO) (Nern et al., 2015), a genetic method capable of sparsely labeling individual cells of a neuronal population in multiple colors. 0–1-day old adult flies were heat shocked for 12-13 minutes to induce sparse labeling of LPLC1 or LPLC2.

Immunohistochemistry

All dissections were performed in ice-cold Schneider's insect media (S2, Sigma Aldrich, #S01416) to avoid tissue degradation. Brains were then transferred to a 1% paraformaldehyde (20% PFA, Electron Microscopy Sciences, #15713) in S2 solution and fixed overnight at 4°C while rotating. Fixed brains were quickly rinsed 3 times and then washed 4 x 10 min with

482

483

484

485

486

487

488

489

490

491

492

493

494

495

496

497

498

499

500

501

502

503

phosphate buffered saline (pH 7.4) with 0.5% Triton X-100 (PBST) (Sigma-Aldrich, 9002-93-1). Brains were next blocked with 5% Normal Goat Serum (Gibco, 16210064) in PBST (PBST-NGS) in for at least 1.5 hr while rotating at RT. Brains were incubated with primary antibodies in PBST-NGS overnight at 4°C while rotating and washed 3 x 30 min with PBST the next day. Brains were then incubated with secondary antibodies in PBST-NGS overnight at 4°C while rotating, and again washed 3 x 30 min with PBST the next day. Prior to DylightTM antibody incubation, brains were blocked with 5% Normal Mouse Serum (Invitrogen 31880) in PBST (PBST-NMS) for at least 1.5 hr while rotating at RT. Brains were incubated in DyLight™ antibodies in PBST-NMS overnight at 4°C followed by a minimum of 3 x 30 min PBST washes. After immunostaining, brains were fixed in a 4% PFA in PBS solution for 45 min at RT, followed by 3 x 30 min PBST washes. Brains were then mounted on Poly-L-lysine (Sigma-Aldrich, 25988-63-0) coated glass coverslips (#1.5). Brains were dehydrated in increasing concentrations of ethanol (30%, 50%, 70%, 95%, 100%, 100%) (Decon Labs, 2705HC) for 5 min at each concentration, and then transferred to 100% xylene (Thermofisher scientific, 1330-20-7) for 5 min to clear the brains. Brains were transferred to fresh 100% xylene for another 5 min. Brains were then embedded in DPX (Electron Microscopy Services, 13510) mounting fluid by dropwise application over the affixed brains (\sim 5-7 drops). The coverslip was then inverted over a microscope slide that had two coverslip spacers (#1) affixed to it with UV glue. The DPX medium was left to cure at RT for at least 24 hr before imaging. Immunostaining was performed using the following antibodies: mouse anti-nc82 (1:40, DSHB, RRID: AB 2314866), mouse anti-broad (1:250, DSHB, RRID: AB 528104), rat anti-DYDDDDK (1:200, Novus Biologicals, RRID: NBP1-06712SS), Alexa Fluor 647 goat antimouse (1:400, Thermo Fisher Scientific, RRID: AB 141725), Alexa Fluor 488 goat anti-rat

(1:400, Thermo Fisher Scientific, RRID: AB_2534074), 488 anti-HA DyLight[™] (1:400, Thermo Fisher Scientific, RRID: AB_2533051), and 550 anti-V5 DyLight[™] (1:400, Bio-Rad Antibodies, RRID: MCA1360D550GA).

Confocal Imaging

All fluorescent images were acquired on an Olympus FV1000 confocal microscope with a 60x, 1.42 NA oil immersion objective (UPlanSApo). For any image quantification, acquisition settings and figure brightness and contrast were kept consistent across samples. Otherwise, parameters for acquisition and figure generation were optimally adjusted.

Image Analysis

Analyses of morphological data were performed using custom MATLAB scripts. To quantify axonal volume throughout the z-stack of a confocal image, neuronal signal was first thresholded using FIJI's RenyiEntropy auto thresholding function and then binarized in MATLAB. A region of interest (ROI) was manually drawn and used to restrict axonal quantification to the axons only. The total number of positive pixels was then calculated, and the overall volume was obtained by multiplying the total pixel count by the image voxel size.

To quantify fluorescence within a glomerulus, the middle plane of the glomerulus was first outlined as an ROI according to the Bruchpilot (Brp) stain. Using the ROI, the integrated density signal and area were then taken using the Measure function in Fiji (Schindelin et al., 2012). Corrected total cell fluorescence was then calculated according to the following formula: integrated density – (area * mean fluorescence of background). The Brp stain was also used to visually identify the lobula and lobula plate layers for scoring.

Connectomics Data Analysis

527

528

529

530

531

532

533

534

535

536

537

538

539

540

541

542

543

544

545

546

547

548

549

To determine connectivity partners of LPLC1 and LPLC2 all neurons labeled as LPLC1 (72) and LPLC2 (100) were identified on the right side of the FAFB dataset hosted in the FlyWire codex (version 783; https://codex.flywire.ai/app/search) (Dorkenwald et al., 2022; Matsliah et al., 2024; Schlegel et al., 2023; Zheng et al., 2018). The right side of the brain was selected as the right optic lobe has been extensively characterized, and individual neurons within the fly's visual system have been identified and proofread (Matsliah et al., 2024). Presynaptic inputs to the entire LPLC1 and LPLC2 populations were retrieved using Python and identified from the FAFB dataset utilizing a confidence metric (cleft score) of 30 for individual synapses. For each population, a list of synapses, along with coordinate information, presynaptic neuron ID, postsynaptic neuron ID, and cleft score for each synapse was obtained (Buhmann et al., 2021; Dorkenwald et al., 2022; Heinrich et al., 2018; Zheng et al., 2018). For all analyses of connectivity, only the presynaptic neurons with synapses in the dendritic arbors in the lobula and lobula plate were considered and identified. A total of 30062 unique presynaptic inputs to both the LPLC1 and LPLC2 populations were identified. However, only 29429 of those neurons provided synaptic input to the dendrites in the lobula and lobula plate. Individual neurons that made less than five total synapses to both populations were not identified and were labeled as 'nan'. Neurons that made five or more synapses but were not identified/labeled in the current version of the codex were labeled as unknown. All other neurons were labeled by their appropriate cell type according to the FlyWire codex (Dorkenwald et al., 2022; Matsliah et al., 2024; Schlegel et al., 2023; Zheng et al., 2018). All neurons labeled as 'nan' or unknown were removed from all subsequent analyses. The major synaptic inputs were identified using

percentages of total synapses to LPLC1 dendrites by counting the number of synapses a given population made with LPLC1, considering presynaptic populations with a percentage of total inputs >1% as major synaptic inputs for each population. The same methodology was repeated for the LPLC2 population.

For visual comparisons of synapse locations on two individual LPLC1 (FAFB neuron ID: 720575940644654752) and LPLC2 (FAFB neuron ID:720575940611740569), individual mesh reconstructions and synaptic inputs were plotted using R (R version 4.0.5 (*R: A Language and Environment for Statistical Computing*, 2021)). For representative skeleton reconstructions of presynaptic inputs, the following representative example neurons were selected: Tm5f: 720575940608888843, Tm20: 720575940627542018, Tm4: 720575940625995780, T2: 720575940633643033.

Electrophysiology and Optogenetics

In vivo whole-cell electrophysiology and optogenetic stimulation were performed as described previously (von Reyn et al., 2017). Flies were anesthetized at 4°C with their head and thorax tethered to a polyether ether ketone plate with UV glue (Loctite 3972). The T1 legs were cut at the femur to avoid cleaning of the head. The proboscis was glued in its retracted position to decrease brain movement during the recording. Cuticle and trachea above the LPLC2 population in the right side of the brain were removed and the brain was perfused with standard extracellular saline (NaCl 103 mmol, KCl 3 mmol, TES 5 mmol, trehalose·2H₂O 8 mmol, glucose 10 mmol, NaHCO₃ 26 mmol, NaH₂PO₄ 1 mmol, CaCl₂·2H₂O 1.5 mmol and MgCl₂·6H₂O 4 mmol; (Gouwens and Wilson, 2009)). To maintain a pH of 7.3, extracellular saline was adjusted to 270-275 mOsm and bubbled with 95% O₂/CO₂. All experiments were

performed at room temperature (20-22°C). Localized application of collagenase (0.5% in extracellular saline) with a glass electrode and mechanical pressure was used to break through the brain sheath, providing access to LPLC2 cell bodies. Patch-clamp electrodes (6-9 M Ω) containing intracellular saline (potassium aspartate 140 mmol, KCl 1 mmol, Hepes 10 mmol, EGTA 1 mmol, Na₃GTP 0.5 mmol, MgATP 4 mmol, Alexafluor-568 5 μ mol, 265 mOsm, pH 7.3) were used to target GFP-labeled LPLC2 soma. The membrane voltage was amplified via MultiClamp 700B, digitized (NI-DAQ, National Instruments) at 20 kHz, and low pass-filtered at 6 kHz. Data were obtained using the Wavesurfer (https://wavesurfer.janelia.org/) open-source software running in MATLAB (MathWorks). Recordings were not adjusted for a 13mV liquid junction potential (Gouwens and Wilson, 2009). For recordings to be considered acceptable, an initial seal resistance of >2 G Ω before rupture and a resting membrane potential of -38 mV was required.

For optogenetic experiments, light was delivered (635 nm LED, Scientifica) through a 40x objective. Light activation (100 ms) of T2 cell types expressing CsChrimson was delivered 5 times at 30 second intervals with 3 repetitions, and recordings were taken from LPLC2 cells.

Electrophysiological Analysis

Analyses of LPLC2 membrane potential peak responses and response latency with respect to the start of the optogenetic light pulse were performed using custom MATLAB scripts. The peak magnitude of the LPLC2 response was measured during the light pulse after baseline (taken one second prior to the light pulse) subtracting the data. Activation latency was measured as the time at which the LPLC2 response exceeded 3 standard deviations of the baseline following optogenetic light stimulation.

Single-cell Perturb-Seq experiment

Virgin females expressing a nuclear GFP reporter (UAS-His2A-GFP) and either *broad* overexpression constructs or a control (empty) chromosome were crossed to males carrying an LPLC2 split-GAL4 driver (OL0048b), as well as a unique isogenic wild-type X-chromosome from the *Drosophila* Reference Genetic Panel (DRGP) (Huang et al., 2014; Mackay et al., 2012). Each experimental condition was crossed to 3-5 unique DGRP genotypes (see Figure 5 for details). F1 generation females were collected at 0h APF and incubated for either 48h or 72h APF.

All brains were dissected and collected in two Eppendorf tubes kept on ice, one for each timepoint (each timepoint was processed as a separate sample). Brains were incubated in a papain (Worthington #LK003178) and protease (Sigma-Aldrich #5401119001) cocktail at 25°C for 30 min, gently washed twice with PBS, then washed with 0.04% BSA in PBS and dissociated mechanically by pipetting. The resulting cell suspension was filtered through a 20 µm cell-strainer (Corning #352235) and sorted by FACS (BD FACS Aria II) to isolate GFP-positive single cells and measure cell concentrations.

Single-cell suspensions were used to generate scRNA-Seq libraries using the 10X Genomics Chromium Next GEM Single Cell 3'-kit (v3.1) following the manufacturer's protocol. Each sample (timepoint) was loaded to a single lane of 10X Chromium with a targeted capture rate of 1,500 cells per sample. Two scRNA-Seq libraries were sequenced using one lane of NovaSeq 6000 SP platform (28bp + 91 bp).

Single-cell RNA-Seq data processing

620

621

622

623

624

625

626

627

628

629

630

631

632

633

634

635

636

637

638

639

640

Raw reads were processed using 10X Cell Ranger (7.1.0) using the reference genome and transcriptome from FlyBase (release 6.29, (Gramates et al., 2022)). The reference genome and transcriptome were appended with the sequence of UAS-His2A-GFP reporter construct to quantify the levels of transgene expression. Single-cell transcriptomes from individual DGRP-marked biological replicates were demultiplexed based on genotypes of their unique DGRP X-chromosomes using demuxlet (version 2, https://github.com/statgen/popscle; (Kang et al., 2018)). The genotypes of DGRP strains (Huang et al., 2014; Mackay et al., 2012) were preprocessed as described in (Kurmangaliyev et al., 2020). Demultiplexing was based on genetic variants from 18 DGRP strains: 15 strains used in the experiment (not all genotypes yielded high-quality transcriptomes) and 3 strains as negative controls. Variants were filtered using the following criteria: (1) only biallelic single-nucleotide polymorphisms (SNP) on X chromosome; (2) SNPs called in all 18 strains (no missing data); (3) non-reference allele only in one of 18 strains. Since we do not have information about the exact genotypes of common maternal chromosomes in F1 heterozygotes, we have quantified allelic coverages of filtered SNPs using samtools mpileup (version 1.10; (Li, 2011)). In heterozygous F1 progeny, the non-reference alleles on a common maternal chromosome are expected to have an allelic frequency of 0.5. Therefore, we only kept SNPs with a minimum coverage of 10 reads and a maximum non-reference allele frequency of 0.25. The resulting set of filtered DGRP SNPs was converted to heterozygous variants using a reference allele as a maternal genotype. In total, 6,765 SNPs were used for demultiplexing. Few cells were incorrectly assigned to the genotypes that were not used in the experiments (negative controls) confirming the accuracy of the demultiplexing step: in the 48h sample, 9 of 1484 cells were

assigned to negative controls (244 were "doublets/ambiguous"); in the 72h sample, 18 of 1101 cells were assigned to the negative controls (138 were "doublets/ambiguous").

Single-cell RNA-seq data analysis

641

642

643

644

645

646

647

648

649

650

651

652

653

654

655

656

657

658

659

660

661

662

663

Single-cell data analysis was performed using Seurat (5.0.1, (Hao et al., 2024)). Each sample (timepoint) was analyzed separately. We kept only high-quality single-cell transcriptomes that were assigned to the expected DGRP genotypes: (UMI/cell: minimum = 10,000, maximum = 50,000; mitochondrial transcripts < 10%). The final datasets included 934 cells for 48h APF and 818 cells for 72h APF. Cells were clustered using the standard Seurat pipeline with default parameters. Total numbers of UMI-per-cell were regressed out at the scaling step (function: ScaleData). Scaled expression values of 2000 highly variable genes were used for principal component analysis, and the first 7 principal components were used for a SNN-based (shared nearest neighbor) clustering (functions: FindNeighbors/FindClusters, resolution = 0.1). The same principal components were used to compute tSNE (t-Distributed Stochastic Neighbor) embeddings. t-SNE plots were used only for the visualization of datasets. Clusters corresponding to LPLC2 neurons were annotated based on the expression of known marker genes (Figure 5). The transcriptional profiles of LPLC2 neurons from the Perturb-Seq experiment were compared to the transcriptional profiles of LPLC1 and LPLC2 neurons in the single-cell atlas of the developing *Drosophila* visual system (Kurmangaliyev et al., 2020). The comparison was based on differentially expressed genes (DEGs) between LPLC1 and LPLC2 at 48h APF (there

were too few LPLC1/LPLC2 cells in the atlas at 72h APF for a meaningful analysis). DEGs were

identified using a Wilcoxon rank-sum test (function: FindMarkers, min.pct = 0.5, min.diff.pct =

665

666

667

668

669

670

671

672

673

674

675

676

677

678

679

680

681

682

683

684

685

686

0.5, pseudocount.use = 0.1). DEGs were filtered using the following criteria: adjusted p-value < 0.01, fold-change > 4, and average normalized expression level > 2 (either in LPLC1 or LPLC2 neurons at 48h APF). The log-scaled average expression profiles of the identified DEGs were compared between LPLC2 neurons in each experimental group in Perturb-Seq and LPLC1/LPLC2 clusters in the atlas using Pearson's correlation coefficients (Figure 5). Expression patterns of genes of interest were visualized using heatmaps. The normalized expression values (transcripts-per-10,000, TP10K) were averaged at the levels of cell types, experimental groups, and/or replicates. The average expression values were log1p-transformed and capped at the maximum value of 20 (3 in log-space). The expression of transcription factors in LPLC1 and LPLC2 neurons in Figure 1c is shown for genes with a minimum expression value of 5 in any of the timepoints. Isoform analysis of atlas and Perturb-seq data The differential use of broad isoforms was visualized using read coverages at the 3'-UTR region of the gene. Reads corresponding to specific cell types, experimental groups, and time points were extracted from the Cell Ranger output bam-files using Sinto (https://github.com/timoast/sinto), quantified using deepTools2 (Ramirez et al., 2016), and visualized using Integrative genomics viewer (IGV) (Robinson et al., 2011). **Statistical Analysis** All boxplots were formatted where the dividing line inside the box indicates the median, the grey boxes contain the interquartile range, and the whiskers indicate the data points that fall

within 1.5x the interquartile range. Outliers were denoted with a + sign.

Statistical tests were selected based on data distribution (Kolmogorov-Smirnov test, 687 MATLAB) and sample size. All statistical tests are as stated in the figure captions. 688 689 **Data and Software Availability** 690 Information about and requests for data can be directed to and will be fulfilled by the 691 Lead Contact, Catherine R. von Reyn. The single-cell transcriptional atlas of the *Drosophila* 692 visual system is available on NCBI GEO (GSE156455) and Zenodo (8111612). The Perturb-Seq 693 dataset will be available on NCBI GEO and Zenodo upon publication. 694 695 **Additional Resources** 696 Immunohistochemistry protocols for driver expression visualization and Multi-Color Flip 697 Out: https://www.janelia.org/project-team/flylight/protocols. 698 699 **Author Contributions** 700 Conceptualization: N.S., M.D., Y.Z.K., and C.R.v.R. 701 Data curation: N.S., M.D., B.W.H, A.M-S., J.A., Y.Z.K., and C.R.v.R. 702 703 Formal Analysis: N.S., B.W.H, A.M-S., R.G., and Y.Z.K. Funding acquisition: J.A., M.D. and C.R.v.R. 704 705 Investigation: N.S., M.D., B.W.H., A.M-S., R.G., C.R.C., A.R., R.H.H., and P.M. 706 Methodology: N.S., M.D., Y.Z.K., and C.R.v.R. Software: N.S., B.W.H., A.M-S., R.G., and Y.Z.K. 707 708 Supervision: J.A., Y.Z.K. and C.R.v.R. 709 Visualization: N.S., B.W.H., A.M-S., Y.Z.K., and C.R.v.R.

710 Writing – original draft: N.S., Y.Z.K., and C.R.v.R. Writing – review & editing: N.S., M.D., B.W.H., A.M-S., J.A., Y.Z.K. and C.R.v.R. 711 712 **Acknowledgments** 713 We thank all current and past members of the von Reyn and Ausborn laboratories for their 714 discussion of this work. We also thank Larry Zipursky for the use of his laboratory to perform 715 the Perturb-seq experiment. This work was supported by the National Science Foundation Grant 716 No. IOS-1921065 (C.R.v.R.), the National Institutes of Health NINDS R01NS118562 (J.A. & 717 718 C.R.v.R.), and the HHMI-Helen Hay Whitney Foundation Fellowship (M.D.). 719 720 721 References Ache, J. M., Polsky, J., Alghailani, S., Parekh, R., Breads, P., Peek, M. Y., Bock, D. D., von 722 Reyn, C. R., & Card, G. M. (2019). Neural Basis for Looming Size and Velocity 723 Encoding in the Drosophila Giant Fiber Escape Pathway. Curr Biol, 29(6), 1073-1081 724 e1074. https://doi.org/10.1016/j.cub.2019.01.079 725 726 Ahn, S., Yang, H., Son, S., Lee, H. S., Park, D., Yim, H., Choi, H. J., Swoboda, P., & Lee, J. (2022). The C. elegans regulatory factor X (RFX) DAF-19M module: A shift from 727 general ciliogenesis to cell-specific ciliary and behavioral specialization. Cell Rep. 39(2), 728 729 110661. https://doi.org/10.1016/j.celrep.2022.110661 Allan, D. W., & Thor, S. (2015). Transcriptional selectors, masters, and combinatorial codes: 730 regulatory principles of neural subtype specification. Wiley Interdiscip Rev Dev Biol, 731 732 4(5), 505-528. https://doi.org/10.1002/wdev.191

733 Arber, S., Han, B., Mendelsohn, M., Smith, M., Jessell, T. M., & Sockanathan, S. (1999). Requirement for the homeobox gene Hb9 in the consolidation of motor neuron identity. 734 Neuron, 23(4), 659-674. https://doi.org/10.1016/s0896-6273(01)80026-x 735 736 Bayer, C. A., Holley, B., & Fristrom, J. W. (1996). A switch in broad-complex zinc-finger 737 isoform expression is regulated posttranscriptionally during the metamorphosis of 738 Drosophila imaginal discs. Dev Biol, 177(1), 1-14. https://doi.org/10.1006/dbio.1996.0140 739 Bayer, C. A., von Kalm, L., & Fristrom, J. W. (1997). Relationships between protein isoforms 740 741 and genetic functions demonstrate functional redundancy at the Broad-Complex during Drosophila metamorphosis. Dev Biol, 187(2), 267-282. 742 https://doi.org/10.1006/dbio.1997.8620 743 Belyaeva, E. S., Aizenzon, M. G., Semeshin, V. F., Kiss, II, Koczka, K., Baritcheva, E. M., 744 Gorelova, T. D., & Zhimulev, I. F. (1980). Cytogenetic analysis of the 2B3-4--2B11 745 region of the X-chromosome of Drosophila melanogaster. I. Cytology of the region and 746 mutant complementation groups. *Chromosoma*, 81(2), 281-306. 747 https://doi.org/10.1007/BF00285954 748 749 Brennan, C. A., Li, T. R., Bender, M., Hsiung, F., & Moses, K. (2001). Broad-complex, but not ecdysone receptor, is required for progression of the morphogenetic furrow in the 750 Drosophila eye. *Development*, 128(1), 1-11. https://doi.org/10.1242/dev.128.1.1 751 752 Buhmann, J., Sheridan, A., Malin-Mayor, C., Schlegel, P., Gerhard, S., Kazimiers, T., Krause, R., Nguyen, T. M., Heinrich, L., Lee, W. A., Wilson, R., Saalfeld, S., Jefferis, G., Bock, 753 D. D., Turaga, S. C., Cook, M., & Funke, J. (2021). Automatic detection of synaptic 754

755 partners in a whole-brain Drosophila electron microscopy data set. *Nat Methods*, 18(7), 771-774. https://doi.org/10.1038/s41592-021-01183-7 756 Campbell, R. F., & Walthall, W. W. (2016). Meis/UNC-62 isoform dependent regulation of 757 CoupTF-II/UNC-55 and GABAergic motor neuron subtype differentiation. Dev Biol. 758 419(2), 250-261. https://doi.org/10.1016/j.ydbio.2016.09.009 759 760 Chao, H. T., Davids, M., Burke, E., Pappas, J. G., Rosenfeld, J. A., McCarty, A. J., Davis, T., Wolfe, L., Toro, C., Tifft, C., Xia, F., Stong, N., Johnson, T. K., Warr, C. G., 761 Undiagnosed Diseases, N., Yamamoto, S., Adams, D. R., Markello, T. C., Gahl, W. A., 762 Bellen, H. J., Wangler, M. F., & Malicdan, M. C. V. (2017). A Syndromic 763 Neurodevelopmental Disorder Caused by De Novo Variants in EBF3. Am J Hum Genet, 764 100(1), 128-137. https://doi.org/10.1016/j.ajhg.2016.11.018 765 766 Chen, Y. C., & Konstantinides, N. (2022). Integration of Spatial and Temporal Patterning in the Invertebrate and Vertebrate Nervous System. Front Neurosci, 16, 854422. 767 https://doi.org/10.3389/fnins.2022.854422 768 Chu, S. Y., Lai, Y. W., Hsu, T. C., Lu, T. M., & Yu, H. H. (2024). Isoforms of Terminal Selector 769 Mamo Control Axon Segregation During Adult Drosophila Memory Center Construction 770 771 Via Semaphorin-1a. https://doi.org/10.2139/ssrn.4749745 Crossgrove, K., Bayer, C. A., Fristrom, J. W., & Guild, G. M. (1996). The Drosophila Broad-772 Complex early gene directly regulates late gene transcription during the ecdysone-773 774 induced puffing cascade. Dev Biol, 180(2), 745-758. https://doi.org/10.1006/dbio.1996.0343 775

776 Davis, F. P., Nern, A., Picard, S., Reiser, M. B., Rubin, G. M., Eddy, S. R., & Henry, G. L. (2020). A genetic, genomic, and computational resource for exploring neural circuit 777 function. Elife, 9. https://doi.org/10.7554/eLife.50901 778 779 Deneris, E. S., & Hobert, O. (2014). Maintenance of postmitotic neuronal cell identity. *Nat* Neurosci, 17(7), 899-907. https://doi.org/10.1038/nn.3731 780 DiBello, P. R., Withers, D. A., Bayer, C. A., Fristrom, J. W., & Guild, G. M. (1991). The 781 Drosophila Broad-Complex encodes a family of related proteins containing zinc fingers. 782 Genetics, 129(2), 385-397. https://doi.org/10.1093/genetics/129.2.385 783 Dionne, H., Hibbard, K. L., Cavallaro, A., Kao, J. C., & Rubin, G. M. (2018). Genetic Reagents 784 for Making Split-GAL4 Lines in Drosophila. Genetics, 209(1), 31-35. 785 https://doi.org/10.1534/genetics.118.300682 786 787 Dorkenwald, S., McKellar, C. E., Macrina, T., Kemnitz, N., Lee, K., Lu, R., Wu, J., Popovych, S., Mitchell, E., Nehoran, B., Jia, Z., Bae, J. A., Mu, S., Ih, D., Castro, M., Ogedengbe, 788 O., Halageri, A., Kuehner, K., Sterling, A. R., Ashwood, Z., Zung, J., Brittain, D., 789 Collman, F., Schneider-Mizell, C., Jordan, C., Silversmith, W., Baker, C., Deutsch, D., 790 Encarnacion-Rivera, L., Kumar, S., Burke, A., Bland, D., Gager, J., Hebditch, J., 791 792 Koolman, S., Moore, M., Morejohn, S., Silverman, B., Willie, K., Willie, R., Yu, S. C., Murthy, M., & Seung, H. S. (2022). FlyWire: online community for whole-brain 793 connectomics. Nat Methods, 19(1), 119-128. https://doi.org/10.1038/s41592-021-01330-0 794 El-Danaf, R. N., Rajesh, R., & Desplan, C. (2023). Temporal regulation of neural diversity in 795 Drosophila and vertebrates. Semin Cell Dev Biol, 142, 13-22. 796 797 https://doi.org/10.1016/j.semcdb.2022.05.011

798

799

800

801

802

803

804

805

806

807

808

809

810

811

812

813

814

815

816

817

818

819

Emery, I. F., Bedian, V., & Guild, G. M. (1994). Differential expression of Broad-Complex transcription factors may forecast tissue-specific developmental fates during Drosophila metamorphosis. Development, 120(11), 3275-3287. https://doi.org/10.1242/dev.120.11.3275 Fischbach, K. F., & Dittrich, A. P. (1989). The optic lobe of Drosophila melanogaster. I. A Golgi analysis of wild-type structure. Cell and Tissue Research, 258, 441-475. https://doi.org/ttps://doi.org/10.1007/BF00218858 Flames, N., & Hobert, O. (2009). Gene regulatory logic of dopamine neuron differentiation. Nature, 458(7240), 885-889. https://doi.org/10.1038/nature07929 Gramates, L. S., Agapite, J., Attrill, H., Calvi, B. R., Crosby, M. A., Dos Santos, G., Goodman, J. L., Goutte-Gattat, D., Jenkins, V. K., Kaufman, T., Larkin, A., Matthews, B. B., Millburn, G., Strelets, V. B., & the FlyBase, C. (2022). FlyBase: a guided tour of highlighted features. Genetics, 220(4). https://doi.org/10.1093/genetics/iyac035 Hao, Y., Stuart, T., Kowalski, M. H., Choudhary, S., Hoffman, P., Hartman, A., Srivastava, A., Molla, G., Madad, S., Fernandez-Granda, C., & Satija, R. (2024). Dictionary learning for integrative, multimodal and scalable single-cell analysis. *Nat Biotechnol*, 42(2), 293-304. https://doi.org/10.1038/s41587-023-01767-y Hassan, B. A., & Hiesinger, P. R. (2015). Beyond Molecular Codes: Simple Rules to Wire Complex Brains. Cell, 163(2), 285-291. https://doi.org/10.1016/j.cell.2015.09.031 Heinrich, L., Funke, J., Pape, C., Nunez-Iglesias, J., & Saalfeld, S. (2018). Synaptic Cleft Segmentation in Non-isotropic Volume Electron Microscopy of the Complete Drosophila Brain. MICCAI 2018,

820 Hobert, O. (2008). Regulatory logic of neuronal diversity: Terminal selector genes and selector motifs. Proceedings of the National Academy of Sciences, 105(51), 20067-20071. 821 https://doi.org/doi:10.1073/pnas.0806070105 822 Hobert, O. (2016). Terminal Selectors of Neuronal Identity. Curr Top Dev Biol, 116, 455-475. 823 https://doi.org/10.1016/bs.ctdb.2015.12.007 824 Hobert, O. (2021). Homeobox genes and the specification of neuronal identity. Nat Rev 825 Neurosci, 22(10), 627-636. https://doi.org/10.1038/s41583-021-00497-x 826 Hobert, O., & Kratsios, P. (2019). Neuronal identity control by terminal selectors in worms, flies, 827 and chordates. Curr Opin Neurobiol, 56, 97-105. 828 https://doi.org/10.1016/j.conb.2018.12.006 829 Holguera, I., & Desplan, C. (2018). Neuronal specification in space and time. Science, 830 362(6411), 176-180. https://doi.org/10.1126/science.aas9435 831 Holmberg, J., & Perlmann, T. (2012). Maintaining differentiated cellular identity. *Nat Rev Genet*, 832 833 13(6), 429-439. https://doi.org/10.1038/nrg3209 Huang, W., Massouras, A., Inoue, Y., Peiffer, J., Ramia, M., Tarone, A. M., Turlapati, L., 834 Zichner, T., Zhu, D., Lyman, R. F., Magwire, M. M., Blankenburg, K., Carbone, M. A., 835 836 Chang, K., Ellis, L. L., Fernandez, S., Han, Y., Highnam, G., Hjelmen, C. E., Jack, J. R., Javaid, M., Jayaseelan, J., Kalra, D., Lee, S., Lewis, L., Munidasa, M., Ongeri, F., Patel, 837 838 S., Perales, L., Perez, A., Pu, L., Rollmann, S. M., Ruth, R., Saada, N., Warner, C., 839 Williams, A., Wu, Y. Q., Yamamoto, A., Zhang, Y., Zhu, Y., Anholt, R. R., Korbel, J. O., Mittelman, D., Muzny, D. M., Gibbs, R. A., Barbadilla, A., Johnston, J. S., Stone, E. 840 A., Richards, S., Deplancke, B., & Mackay, T. F. (2014). Natural variation in genome 841

architecture among 205 Drosophila melanogaster Genetic Reference Panel lines. Genome 842 Res, 24(7), 1193-1208. https://doi.org/10.1101/gr.171546.113 843 Huet, F., Ruiz, C., & Richards, G. (1993). Puffs and PCR: the in vivo dynamics of early gene 844 expression during ecdysone responses in Drosophila. Development, 118(2), 613-627. 845 https://doi.org/10.1242/dev.118.2.613 846 Jain, S., Lin, Y., Kurmangaliyev, Y. Z., Valdes-Aleman, J., LoCascio, S. A., Mirshahidi, P., 847 Parrington, B., & Zipursky, S. L. (2022). A global timing mechanism regulates cell-type-848 specific wiring programmes. Nature, 603(7899), 112-118. 849 850 https://doi.org/10.1038/s41586-022-04418-5 851 Jenett, A., Rubin, G. M., Ngo, T. T., Shepherd, D., Murphy, C., Dionne, H., Pfeiffer, B. D., Cavallaro, A., Hall, D., Jeter, J., Iyer, N., Fetter, D., Hausenfluck, J. H., Peng, H., 852 Trautman, E. T., Svirskas, R. R., Myers, E. W., Iwinski, Z. R., Aso, Y., DePasquale, G. 853 M., Enos, A., Hulamm, P., Lam, S. C., Li, H. H., Laverty, T. R., Long, F., Qu, L., 854 Murphy, S. D., Rokicki, K., Safford, T., Shaw, K., Simpson, J. H., Sowell, A., Tae, S., 855 Yu, Y., & Zugates, C. T. (2012). A GAL4-driver line resource for Drosophila 856 neurobiology. Cell Rep. 2(4), 991-1001. https://doi.org/10.1016/j.celrep.2012.09.011 857 858 Kang, H. M., Subramaniam, M., Targ, S., Nguyen, M., Maliskova, L., McCarthy, E., Wan, E., Wong, S., Byrnes, L., Lanata, C. M., Gate, R. E., Mostafavi, S., Marson, A., Zaitlen, N., 859 Criswell, L. A., & Ye, C. J. (2018). Multiplexed droplet single-cell RNA-sequencing 860 861 using natural genetic variation. *Nat Biotechnol*, 36(1), 89-94. https://doi.org/10.1038/nbt.4042 862

863

864

865

866

867

868

869

870

871

872

873

874

875

876

877

878

879

880

881

882

883

884

Karim, F. D., Guild, G. M., & Thummel, C. S. (1993). The Drosophila Broad-Complex plays a key role in controlling ecdysone-regulated gene expression at the onset of metamorphosis. Development, 118(3), 977-988, https://doi.org/10.1242/dev.118.3.977 Kiss, I., Beaton, A. H., Tardiff, J., Fristrom, D., & Fristrom, J. W. (1988). Interactions and developmental effects of mutations in the Broad-Complex of Drosophila melanogaster. Genetics, 118(2), 247-259. https://doi.org/10.1093/genetics/118.2.247 Kiss, I., Bencze, G., Fodor, G., Szabad, J., & Fristrom, J. W. (1976). Prepupal larval mosaics in Drosophila melanogaster, *Nature*, 262(5564), 136-138, https://doi.org/10.1038/262136a0 Klapoetke, N. C., Nern, A., Peek, M. Y., Rogers, E. M., Breads, P., Rubin, G. M., Reiser, M. B., & Card, G. M. (2017). Ultra-selective looming detection from radial motion opponency. *Nature*, 551(7679), 237-241. https://doi.org/10.1038/nature24626 Klapoetke, N. C., Nern, A., Rogers, E. M., Rubin, G. M., Reiser, M. B., & Card, G. M. (2022), A functionally ordered visual feature map in the Drosophila brain. *Neuron*. https://doi.org/10.1016/j.neuron.2022.02.013 Konstantinides, N., Kapuralin, K., Fadil, C., Barboza, L., Satija, R., & Desplan, C. (2018). Phenotypic Convergence: Distinct Transcription Factors Regulate Common Terminal Features. Cell, 174(3), 622-635 e613. https://doi.org/10.1016/j.cell.2018.05.021 Kumar, J. P. (2001). Signalling pathways in Drosophila and vertebrate retinal development. *Nat* Rev Genet, 2(11), 846-857. https://doi.org/10.1038/35098564 Kurmangaliyev, Y. Z., Yoo, J., Valdes-Aleman, J., Sanfilippo, P., & Zipursky, S. L. (2020). Transcriptional Programs of Circuit Assembly in the Drosophila Visual System. *Neuron*,

108(6), 1045-1057 e1046. https://doi.org/10.1016/j.neuron.2020.10.006

Lai, S. L., & Lee, T. (2006). Genetic mosaic with dual binary transcriptional systems in 885 Drosophila. *Nat Neurosci*, 9(5), 703-709. https://doi.org/10.1038/nn1681 886 Li, H. (2011). A statistical framework for SNP calling, mutation discovery, association mapping 887 and population genetical parameter estimation from sequencing data. *Bioinformatics*, 888 27(21), 2987-2993. https://doi.org/10.1093/bioinformatics/btr509 889 Li, X., Erclik, T., Bertet, C., Chen, Z., Voutev, R., Venkatesh, S., Morante, J., Celik, A., & 890 Desplan, C. (2013). Temporal patterning of Drosophila medulla neuroblasts controls 891 neural fates. *Nature*, 498(7455), 456-462. https://doi.org/10.1038/nature12319 892 893 Mackay, T. F., Richards, S., Stone, E. A., Barbadilla, A., Ayroles, J. F., Zhu, D., Casillas, S., Han, Y., Magwire, M. M., Cridland, J. M., Richardson, M. F., Anholt, R. R., Barron, M., 894 Bess, C., Blankenburg, K. P., Carbone, M. A., Castellano, D., Chaboub, L., Duncan, L., 895 Harris, Z., Javaid, M., Jayaseelan, J. C., Jhangiani, S. N., Jordan, K. W., Lara, F., 896 Lawrence, F., Lee, S. L., Librado, P., Linheiro, R. S., Lyman, R. F., Mackey, A. J., 897 Munidasa, M., Muzny, D. M., Nazareth, L., Newsham, I., Perales, L., Pu, L. L., Qu, C., 898 Ramia, M., Reid, J. G., Rollmann, S. M., Rozas, J., Saada, N., Turlapati, L., Worley, K. 899 C., Wu, Y. Q., Yamamoto, A., Zhu, Y., Bergman, C. M., Thornton, K. R., Mittelman, D., 900 901 & Gibbs, R. A. (2012). The Drosophila melanogaster Genetic Reference Panel. *Nature*, 482(7384), 173-178. https://doi.org/10.1038/nature10811 902 Makos, M. A., Kuklinski, N. J., Berglund, E. C., Heien, M. L., & Ewing, A. G. (2009). Chemical 903 904 measurements in Drosophila. Trends Analyt Chem, 28(11), 1223-1234. https://doi.org/10.1016/j.trac.2009.08.005 905 906 Matsliah, Szi-chieh Yu, Krzysztof Kruk, Doug Bland, Austin Burke, Jay Gager, James Hebditch, Ben Silverman, Kyle Willie, Ryan Willie, Marissa Sorek, Amy R. Sterling, Emil Kind, 907

908 Dustin Garner, Gizem Sancer, Mathias F. Wernet, Sung Soo Kim, Mala Murthy, H. Sebastian Seung, & Consortium, t. F. (2024). Neuronal "parts list" and wiring diagram 909 for a visual system, https://doi.org/https://doi.org/10.1101/2023.10.12.562119 910 McFarland, B. W., Smolin, N., Jang, H., Hina, B. W., Parisi, M. J., Davis, K. C., Mosca, T. J., 911 Godenschewege, T. A., Nern, A., Kurmangaliyev, Y. Z., & von Reyn, C. R. (2024). 912 Axon arrival times and physical occupancy establish visual projection neuron integration 913 on developing dendrites in the Drosophila optic glomeruli. *Elife*, 13:RP96223. 914 https://doi.org/https://doi.org/10.7554/eLife.96223.1 915 916 Miller, J., McLachlan, A. D., & Klug, A. (1985). Repetitive zinc-binding domains in the protein transcription factor IIIA from Xenopus oocytes. EMBO J, 4(6), 1609-1614. 917 https://doi.org/10.1002/j.1460-2075.1985.tb03825.x 918 919 Mugat, B., Brodu, V., Keizlarova-Lepesant, J., Antoniewski, C., Baver, C. A., Fristrom, J. W., & Lepesant, J. A. (2000). Dynamic expression of broad-complex isoforms mediates 920 temporal control of an ecdysteroid target gene at the onset of Drosophila metamorphosis. 921 Dev Biol, 227(1), 104-117. https://doi.org/10.1006/dbio.2000.9879 922 Nern, A., Loesche, F., Takemura, S. Y., Burnett, L. E., Dreher, M., Gruntman, E., Hoeller, J., 923 924 Huang, G. B., Januszewski, M., Klapoetke, N. C., Koskela, S., Longden, K. D., Lu, Z., Preibisch, S., Qiu, W., Rogers, E. M., Seenivasan, P., Zhao, A., Bogovic, J., Canino, B. 925 S., Clements, J., Cook, M., Finley-May, S., Flynn, M. A., Fragniere, A. M., Hameed, I., 926 927 Hayworth, K. J., Hopkins, G. P., Hubbard, P. M., Katz, W. T., Kovalyak, J., Lauchie, S. A., Leonard, M., Lohff, A., Maldonado, C. A., Mooney, C., Okeoma, N., Olbris, D. J., 928 Ordish, C., Paterson, T., Phillips, E. M., Pietzsch, T., Rivas Salinas, J., Rivlin, P. K., 929 930 Schlegel, P., Scott, A. L., Scuderi, L. A., Takemura, S., Talebi, I., Thomson, A.,

931 Trautman, E. T., Umayam, L., Walsh, C., Walsh, J. J., Xu, C. S., Yakal, E. A., Yang, T., Zhao, T., Funke, J., George, R., Hess, H. F., Jefferis, G., Knecht, C., Korff, W., Plaza, S. 932 M., Romani, S., Saalfeld, S., Scheffer, L. K., Berg, S., Rubin, G. M., & Reiser, M. B. 933 (2024). Connectome-driven neural inventory of a complete visual system. bioRxiv. 934 https://doi.org/10.1101/2024.04.16.589741 935 Nern, A., Pfeiffer, B. D., & Rubin, G. M. (2015). Optimized tools for multicolor stochastic 936 labeling reveal diverse stereotyped cell arrangements in the fly visual system. Proc Natl 937 Acad Sci U S A, 112(22), E2967-2976. https://doi.org/10.1073/pnas.1506763112 938 939 Neville, M. C., Nojima, T., Ashley, E., Parker, D. J., Walker, J., Southall, T., Van de Sande, B., Marques, A. C., Fischer, B., Brand, A. H., Russell, S., Ritchie, M. G., Aerts, S., & 940 Goodwin, S. F. (2014). Male-specific fruitless isoforms target neurodevelopmental genes 941 to specify a sexually dimorphic nervous system. Curr Biol, 24(3), 229-241. 942 https://doi.org/10.1016/j.cub.2013.11.035 943 O'Meara, M. M., Zhang, F., & Hobert, O. (2010). Maintenance of neuronal laterality in 944 Caenorhabditis elegans through MYST histone acetyltransferase complex components 945 LSY-12, LSY-13 and LIN-49. Genetics, 186(4), 1497-1502. 946 947 https://doi.org/10.1534/genetics.110.123661 Ozel, M. N., Gibbs, C. S., Holguera, I., Soliman, M., Bonneau, R., & Desplan, C. (2022). 948 Coordinated control of neuronal differentiation and wiring by sustained transcription 949 950 factors. Science, 378(6626), eadd1884. https://doi.org/10.1126/science.add1884 Ozel, M. N., Simon, F., Jafari, S., Holguera, I., Chen, Y. C., Benhra, N., El-Danaf, R. N., 951 952 Kapuralin, K., Malin, J. A., Konstantinides, N., & Desplan, C. (2021). Neuronal diversity

and convergence in a visual system developmental atlas. Nature, 589(7840), 88-95. 953 https://doi.org/10.1038/s41586-020-2879-3 954 Pereira, L., Aeschimann, F., Wang, C., Lawson, H., Serrano-Saiz, E., Portman, D. S., Grosshans, 955 H., & Hobert, O. (2019). Timing mechanism of sexually dimorphic nervous system 956 differentiation. *Elife*, 8. https://doi.org/10.7554/eLife.42078 957 958 Perkins, L. A., Holderbaum, L., Tao, R., Hu, Y., Sopko, R., McCall, K., Yang-Zhou, D., Flockhart, I., Binari, R., Shim, H. S., Miller, A., Housden, A., Foos, M., Randkelv, S., 959 Kelley, C., Namgyal, P., Villalta, C., Liu, L. P., Jiang, X., Huan-Huan, Q., Wang, X., 960 961 Fujiyama, A., Toyoda, A., Ayers, K., Blum, A., Czech, B., Neumuller, R., Yan, D., Cavallaro, A., Hibbard, K., Hall, D., Cooley, L., Hannon, G. J., Lehmann, R., Parks, A., 962 Mohr, S. E., Ueda, R., Kondo, S., Ni, J. Q., & Perrimon, N. (2015). The Transgenic 963 RNAi Project at Harvard Medical School: Resources and Validation. *Genetics*, 201(3), 964 843-852. https://doi.org/10.1534/genetics.115.180208 965 Pfeiffer, B. D., Ngo, T. T., Hibbard, K. L., Murphy, C., Jenett, A., Truman, J. W., & Rubin, G. 966 M. (2010). Refinement of tools for targeted gene expression in Drosophila. *Genetics*, 967 186(2), 735-755. https://doi.org/10.1534/genetics.110.119917 968 969 R: A Language and Environment for Statistical Computing. In. (2021). R Foundation for Statistical Computing. https://www.R-project.org/ 970 Ramirez, F., Ryan, D. P., Gruning, B., Bhardwaj, V., Kilpert, F., Richter, A. S., Heyne, S., 971 972 Dundar, F., & Manke, T. (2016). deepTools2: a next generation web server for deepsequencing data analysis. *Nucleic Acids Res*, 44(W1), W160-165. 973 974 https://doi.org/10.1093/nar/gkw257

975 Remesal, L., Roger-Baynat, I., Chirivella, L., Maicas, M., Brocal-Ruiz, R., Perez-Villalba, A., Cucarella, C., Casado, M., & Flames, N. (2020). PBX1 acts as terminal selector for 976 olfactory bulb dopaminergic neurons. Development, 147(8). 977 https://doi.org/10.1242/dev.186841 978 Restifo, L. L., & White, K. (1991). Mutations in a steroid hormone-regulated gene disrupt the 979 metamorphosis of the central nervous system in Drosophila. Dev Biol, 148(1), 174-194. 980 https://doi.org/10.1016/0012-1606(91)90328-z 981 Robinson, J. T., Thorvaldsdottir, H., Winckler, W., Guttman, M., Lander, E. S., Getz, G., & 982 983 Mesirov, J. P. (2011). Integrative genomics viewer. *Nat Biotechnol*, 29(1), 24-26. https://doi.org/10.1038/nbt.1754 984 Sahay, A., & Hen, R. (2007). Adult hippocampal neurogenesis in depression. *Nat Neurosci*, 985 10(9), 1110-1115. https://doi.org/10.1038/nn1969 986 Scheffer, L. K., Xu, C. S., Januszewski, M., Lu, Z., Takemura, S. Y., Hayworth, K. J., Huang, G. 987 B., Shinomiya, K., Maitlin-Shepard, J., Berg, S., Clements, J., Hubbard, P. M., Katz, W. 988 T., Umayam, L., Zhao, T., Ackerman, D., Blakely, T., Bogovic, J., Dolafi, T., 989 Kainmueller, D., Kawase, T., Khairy, K. A., Leavitt, L., Li, P. H., Lindsey, L., Neubarth, 990 991 N., Olbris, D. J., Otsuna, H., Trautman, E. T., Ito, M., Bates, A. S., Goldammer, J., Wolff, T., Svirskas, R., Schlegel, P., Neace, E., Knecht, C. J., Alvarado, C. X., Bailey, D. 992 A., Ballinger, S., Borycz, J. A., Canino, B. S., Cheatham, N., Cook, M., Dreher, M., 993 994 Duclos, O., Eubanks, B., Fairbanks, K., Finley, S., Forknall, N., Francis, A., Hopkins, G. P., Joyce, E. M., Kim, S., Kirk, N. A., Kovalyak, J., Lauchie, S. A., Lohff, A., 995 Maldonado, C., Manley, E. A., McLin, S., Mooney, C., Ndama, M., Ogundeyi, O., 996 997 Okeoma, N., Ordish, C., Padilla, N., Patrick, C. M., Paterson, T., Phillips, E. E., Phillips,

E. M., Rampally, N., Ribeiro, C., Robertson, M. K., Rymer, J. T., Ryan, S. M., Sammons, 998 M., Scott, A. K., Scott, A. L., Shinomiya, A., Smith, C., Smith, K., Smith, N. L., Sobeski, 999 M. A., Suleiman, A., Swift, J., Takemura, S., Talebi, I., Tarnogorska, D., Tenshaw, E., 1000 Tokhi, T., Walsh, J. J., Yang, T., Horne, J. A., Li, F., Parekh, R., Rivlin, P. K., 1001 Jayaraman, V., Costa, M., Jefferis, G. S., Ito, K., Saalfeld, S., George, R., Meinertzhagen, 1002 1003 I. A., Rubin, G. M., Hess, H. F., Jain, V., & Plaza, S. M. (2020). A connectome and analysis of the adult Drosophila central brain. Elife, 9. 1004 https://doi.org/10.7554/eLife.57443 1005 1006 Schindelin, J., Arganda-Carreras, I., Frise, E., Kaynig, V., Longair, M., Pietzsch, T., Preibisch, 1007 S., Rueden, C., Saalfeld, S., Schmid, B., Tinevez, J. Y., White, D. J., Hartenstein, V., Eliceiri, K., Tomancak, P., & Cardona, A. (2012). Fiji: an open-source platform for 1008 biological-image analysis. *Nat Methods*, 9(7), 676-682. 1009 https://doi.org/10.1038/nmeth.2019 1010 Schizophrenia Working Group of the Psychiatric Genomics, C. (2014). Biological insights from 1011 1012 108 schizophrenia-associated genetic loci. *Nature*, 511(7510), 421-427. https://doi.org/10.1038/nature13595 1013 1014 Schlegel, P., Yin, Y., Bates, A. S., Dorkenwald, S., Eichler, K., Brooks, P., Han, D. S., Gkantia, M., Dos Santos, M., Munnelly, E. J., Badalamente, G., Capdevila, L. S., Sane, V. A., 1015 1016 Pleijzier, M. W., Tamimi, I. F. M., Dunne, C. R., Salgarella, I., Javier, A., Fang, S., 1017 Perlman, E., Kazimiers, T., Jagannathan, S. R., Matsliah, A., Sterling, A. R., Yu, S. C., McKellar, C. E., FlyWire, C., Costa, M., Seung, H. S., Murthy, M., Hartenstein, V., 1018 1019 Bock, D. D., & Jefferis, G. (2023). Whole-brain annotation and multi-connectome cell

1020 typing quantifies circuit stereotypy in Drosophila. bioRxiv. 1021 https://doi.org/10.1101/2023.06.27.546055 Serrano-Saiz, E., Poole, R. J., Felton, T., Zhang, F., De La Cruz, E. D., & Hobert, O. (2013). 1022 Modular control of glutamatergic neuronal identity in C. elegans by distinct 1023 homeodomain proteins. Cell, 155(3), 659-673. https://doi.org/10.1016/j.cell.2013.09.052 1024 Sleven, H., Welsh, S. J., Yu, J., Churchill, M. E. A., Wright, C. F., Henderson, A., Horvath, R., 1025 Rankin, J., Vogt, J., Magee, A., McConnell, V., Green, A., King, M. D., Cox, H., 1026 Armstrong, L., Lehman, A., Nelson, T. N., Deciphering Developmental Disorders, s., 1027 study, C., Williams, J., Clouston, P., Hagman, J., & Nemeth, A. H. (2017). De Novo 1028 1029 Mutations in EBF3 Cause a Neurodevelopmental Syndrome. Am J Hum Genet, 100(1), 1030 138-150. https://doi.org/10.1016/j.ajhg.2016.11.020 Takemura, S. Y., Bharioke, A., Lu, Z., Nern, A., Vitaladevuni, S., Rivlin, P. K., Katz, W. T., 1031 Olbris, D. J., Plaza, S. M., Winston, P., Zhao, T., Horne, J. A., Fetter, R. D., Takemura, 1032 S., Blazek, K., Chang, L. A., Ogundevi, O., Saunders, M. A., Shapiro, V., Sigmund, C., 1033 Rubin, G. M., Scheffer, L. K., Meinertzhagen, I. A., & Chklovskii, D. B. (2013). A visual 1034 motion detection circuit suggested by Drosophila connectomics. *Nature*, 500(7461), 175-1035 1036 181. https://doi.org/10.1038/nature12450 Takemura, S. Y., Xu, C. S., Lu, Z., Rivlin, P. K., Parag, T., Olbris, D. J., Plaza, S., Zhao, T., 1037 Katz, W. T., Umayam, L., Weaver, C., Hess, H. F., Horne, J. A., Nunez-Iglesias, J., 1038 1039 Aniceto, R., Chang, L. A., Lauchie, S., Nasca, A., Ogundeyi, O., Sigmund, C., Takemura, S., Tran, J., Langille, C., Le Lacheur, K., McLin, S., Shinomiya, A., Chklovskii, D. B., 1040 Meinertzhagen, I. A., & Scheffer, L. K. (2015). Synaptic circuits and their variations 1041

within different columns in the visual system of Drosophila. Proc Natl Acad Sci USA, 1042 1043 112(44), 13711-13716. https://doi.org/10.1073/pnas.1509820112 Tanaka, R., & Clark, D. A. (2022). Neural mechanisms to exploit positional geometry for 1044 1045 collision avoidance. Curr Biol, 32(11), 2357-2374 e2356. 1046 https://doi.org/10.1016/j.cub.2022.04.023 Tsuchida, T., Ensini, M., Morton, S. B., Baldassare, M., Edlund, T., Jessell, T. M., & Pfaff, S. L. 1047 (1994). Topographic organization of embryonic motor neurons defined by expression of 1048 LIM homeobox genes. Cell, 79(6), 957-970. https://doi.org/10.1016/0092-1049 1050 8674(94)90027-2 von Reyn, C. R., Breads, P., Peek, M. Y., Zheng, G. Z., Williamson, W. R., Yee, A. L., 1051 Leonardo, A., & Card, G. M. (2014). A spike-timing mechanism for action selection. *Nat* 1052 Neurosci, 17(7), 962-970. https://doi.org/10.1038/nn.3741 1053 von Reyn, C. R., Nern, A., Williamson, W. R., Breads, P., Wu, M., Namiki, S., & Card, G. M. 1054 (2017), Feature Integration Drives Probabilistic Behavior in the Drosophila Escape 1055 Response. Neuron, 94(6), 1190-1204 e1196. 1056 https://doi.org/10.1016/j.neuron.2017.05.036 1057 1058 Wolfram, V., Southall, T. D., Gunay, C., Prinz, A. A., Brand, A. H., & Baines, R. A. (2014). The transcription factors islet and Lim3 combinatorially regulate ion channel gene expression. 1059 1060 J Neurosci, 34(7), 2538-2543. https://doi.org/10.1523/JNEUROSCI.4511-13.2014 1061 Wu, M., Nern, A., Williamson, W. R., Morimoto, M. M., Reiser, M. B., Card, G. M., & Rubin, G. M. (2016). Visual projection neurons in the Drosophila lobula link feature detection to 1062 1063 distinct behavioral programs. *Elife*, 5. https://doi.org/10.7554/eLife.21022

1064 Wyler, S. C., Spencer, W. C., Green, N. H., Rood, B. D., Crawford, L., Craige, C., Gresch, P., McMahon, D. G., Beck, S. G., & Deneris, E. (2016). Pet-1 Switches Transcriptional 1065 Targets Postnatally to Regulate Maturation of Serotonin Neuron Excitability. J Neurosci. 1066 1067 36(5), 1758-1774. https://doi.org/10.1523/JNEUROSCI.3798-15.2016 Yao, C., Sasaki, H. M., Ueda, T., Tomari, Y., & Tadakuma, H. (2015). Single-Molecule Analysis 1068 of the Target Cleavage Reaction by the Drosophila RNAi Enzyme Complex. Mol Cell, 1069 59(1), 125-132. https://doi.org/10.1016/j.molcel.2015.05.015 1070 Zheng, Z., Lauritzen, J. S., Perlman, E., Robinson, C. G., Nichols, M., Milkie, D., Torrens, O., 1071 1072 Price, J., Fisher, C. B., Sharifi, N., Calle-Schuler, S. A., Kmecova, L., Ali, I. J., Karsh, B., 1073 Trautman, E. T., Bogovic, J. A., Hanslovsky, P., Jefferis, G., Kazhdan, M., Khairy, K., Saalfeld, S., Fetter, R. D., & Bock, D. D. (2018). A Complete Electron Microscopy 1074 Volume of the Brain of Adult Drosophila melanogaster. *Cell*, 174(3), 730-743 e722. 1075 https://doi.org/10.1016/j.cell.2018.06.019 1076 Zhou, B., Williams, D. W., Altman, J., Riddiford, L. M., & Truman, J. W. (2009). Temporal 1077 1078 patterns of broad isoform expression during the development of neuronal lineages in Drosophila. Neural Dev. 4, 39. https://doi.org/10.1186/1749-8104-4-39 1079 1080